

NAVAL POSTGRADUATE SCHOOL Monterey, California

AD-A199 194



THESIS

DTIC
ELECTE
SEP 13 1988
S D
C&D

FLOW VISUALIZATION OF THE AIRWAKE AROUND A
MODEL OF A TARAWA CLASS LHA IN A SIMULATED
ATMOSPHERIC BOUNDARY LAYER

by

William H. Daley, III

June 1988

Thesis Advisor:

J. Val Healey

Approved for public release; distribution is unlimited

REPORT DOCUMENTATION PAGE

1a REPORT SECURITY CLASSIFICATION UNCLASSIFIED		1b RESTRICTIVE MARKINGS	
2a SECURITY CLASSIFICATION AUTHORITY		3 DISTRIBUTION/AVAILABILITY OF REPORT Approved for public release; distribution is unlimited	
2b DECLASSIFICATION/DOWNGRADING SCHEDULE		5 MONITORING ORGANIZATION REPORT NUMBER(S)	
4 PERFORMING ORGANIZATION REPORT NUMBER(S)		7a NAME OF MONITORING ORGANIZATION Naval Postgraduate School	
6a NAME OF PERFORMING ORGANIZATION Naval Postgraduate School	6b OFFICE SYMBOL (If applicable) Code 67	7b ADDRESS (City, State, and ZIP Code) Monterey, California 93943-5000	
8a NAME OF FUNDING/SPONSORING ORGANIZATION		9 PROCUREMENT INSTRUMENT IDENTIFICATION NUMBER	
8b OFFICE SYMBOL (If applicable)		10 SOURCE OF FUNDING NUMBERS	
8c ADDRESS (City, State, and ZIP Code) Monterey, California 93943-5000		PROGRAM ELEMENT NO	PROJECT NO
		TASK NO	WORK UNIT ACCESSION NO
11 TITLE (Include Security Classification) FLOW VISUALIZATION OF THE AIRWAKE AROUND A MODEL OF A TARAWA CLASS LHA IN A SIMULATED ATMOSPHERIC BOUNDARY LAYER			
12 PERSONAL AUTHOR(S) Daley, William H. III			
13a TYPE OF REPORT Master's Thesis	13b TIME COVERED FROM _____ TO _____	14 DATE OF REPORT (Year, Month, Day) 1988, June	15 PAGE COUNT 95
16 SUPPLEMENTARY NOTATION The views expressed in this thesis are those of the author and do not reflect the official policy or position of the Department of Defense or the U.S. Government.			
17 COSATI CODES		18 SUBJECT TERMS (Continue on reverse if necessary and identify by block number)	
FIELD	GROUP	SUB GROUP	
		Flow Visualization; Simulated Atmospheric Boundary Layer, TARAWA Class LHA	
19 ABSTRACT (Continue on reverse if necessary and identify by block number) A qualitative analysis of the airwake of a TARAWA class LHA in a simulated atmospheric boundary layer was conducted using the environmental wind tunnel, at the Naval Postgraduate School, Monterey, California. Helium bubble flow visualization techniques were employed and a photographic record made of the results. The study utilized a 1:205 scale wooden model of the LHA, suitably mounted to a motion simulator able to fix various combinations of pitch, roll and yaw. Helium bubble flow visualization produced excellent photographic results. Yaw angles of 0° and 30° starboard showed a generally smooth flow pattern with bow trailing vortices, while a yaw angle of 45° port displayed areas of significant turbulence and recirculation zones.			
20 DISTRIBUTION/AVAILABILITY OF ABSTRACT <input checked="" type="checkbox"/> UNCLASSIFIED/UNLIMITED <input type="checkbox"/> SAME AS RPT <input type="checkbox"/> OTIC USERS		21 ABSTRACT SECURITY CLASSIFICATION Unclassified	
22a NAME OF RESPONSIBLE INDIVIDUAL Prof. J. Val Healey		22b TELEPHONE (Include Area Code) (408) 646-2804	22c OFFICE SYMBOL Code 67He

Approved for public release; distribution is unlimited

Flow Visualization of the Airwake Around a Model
of a TARAWA Class LHA in a Simulated
Atmospheric Boundary Layer

by

William H. Daley, III
Lieutenant Commander, United States Navy
B.S., United States Naval Academy, 1975

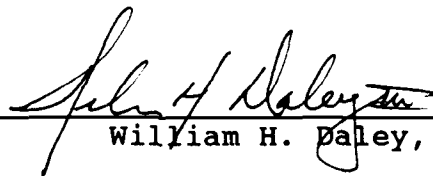
Submitted in partial fulfillment of the
requirements for the degree of

MASTER OF SCIENCE IN AERONAUTICAL ENGINEERING

from the

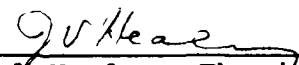
NAVAL POSTGRADUATE SCHOOL
June 1988

Author:

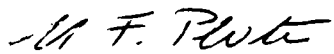


William H. Daley, III


Approved by:



J. Val Healey, Thesis Advisor



M.F. Platzter, Chairman
Department of Aeronautics and Astronautics



Gordon E. Schacher,
Dean of Science and Engineering

ABSTRACT

A qualitative analysis of the airwake of a TARAWA class LHA in a simulated atmospheric boundary layer was conducted using the environmental wind tunnel at the Naval Postgraduate School, Monterey, California. Helium bubble flow visualization techniques were employed and a photographic record made of the results. The study utilized a 1:205 scale wooden model of the LHA, suitably mounted to a motion simulator able to fix various combinations of pitch, roll and yaw. Helium bubble flow visualization produced excellent photographic results. Yaw angles of 0° and 30° starboard showed a generally smooth flow pattern with bow trailing vortices, while a yaw angle of 45° port displayed areas of significant turbulence and recirculation zones.



Accession For	
NTIS GRA&I	<input checked="" type="checkbox"/>
DTIC TAB	<input type="checkbox"/>
Unannounced	<input type="checkbox"/>
Justification	
By	
Distribution	
Availability Codes	
DISTRIBUTION STATEMENT	
A-1	

TABLE OF CONTENTS

I.	INTRODUCTION -----	1
II.	ATMOSPHERIC BOUNDARY LAYER MODELING -----	3
	A. THEORY -----	3
	B. WIND TUNNEL MODELING -----	5
III.	SHIP MOTION -----	13
	A. THEORY -----	13
	B. SHIP MOTION PROGRAM SOFTWARE -----	16
	C. EXPERIMENTAL MODELING -----	17
	D. BLUFF BODY AERODYNAMICS -----	20
IV.	EXPERIMENTAL APPARATUS -----	22
	A. WIND TUNNEL DESCRIPTION -----	22
	B. WIND TUNNEL MODIFICATIONS -----	24
	C. OSCILLATING MECHANISM -----	29
	D. SHIP MODEL -----	31
V.	HELIUM BUBBLE FLOW VISUALIZATION -----	34
	A. BACKGROUND -----	34
	B. HELIUM BUBBLE GENERATION -----	34
	C. PHOTOGRAPHY -----	37
VI.	RESULTS -----	39
	A. ZERO DEGREE YAW -----	44
	B. FORTY-FIVE DEGREE PORT YAW -----	50
	C. THIRTY DEGREE STBD YAW -----	65
VII.	CONCLUSIONS AND RECOMMENDATIONS -----	78

LIST OF REFERENCES -----	81
INITIAL DISTRIBUTION LIST -----	83

LIST OF TABLES

1. SHIP MOTION PARAMETERS -----	20
2. TEST SECTION VELOCITY DATA (ft/sec) -----	27
3. TEST SECTION % TURBULENCE INTENSITY DATA -----	28
4. TARAHA CLASS LHA 1:205 SCALE MODEL -----	33

LIST OF FIGURES

1.	Surface Roughness Parameter z_0 -----	7
2.	The (Longitudinal) Turbulence Intensity -----	8
3.	Values of the Length Scale Parameter L -----	9
4.	Schematic of the Naval Postgraduate School Flow Visualization Tunnel -----	23
5.	NPS Flow Visualization Tunnel -----	25
6.	Ship Model Oscillating Mechanism -----	30
7.	TARAWA Class LHA -----	32
8.	Diagram of the Helium Bubble System -----	35
9.	LHA Flight Deck with Helicopter Spots -----	43
10.	0° Yaw: 0° Pitch, 0° Roll, Bow -----	45
11.	0° Yaw: 0° Pitch, 0° Roll, Midships -----	45
12.	0° Yaw: 0° Pitch, 0° Roll, Stern -----	46
13.	0° Yaw: 1.1° Pitch Up, 0° Roll, Bow -----	46
14.	0° Yaw: 1.1° Pitch Up, 0° Roll, Midships -----	47
15.	0° Yaw: 1.1° Pitch Up, 0° Roll, Stern -----	47
16.	0° Yaw: 0° Pitch, 6° Port Roll, Bow -----	48
17.	0° Yaw: 0° Pitch, 6° Port Roll, Midships -----	48
18.	0° Yaw: 0° Pitch, 6° Port Roll, Stern -----	49
19.	0° Yaw: 1.1° Pitch Up, 6° Port Roll, Bow -----	49
20.	0° Yaw: 1.1° Pitch Up, 6° Port Roll, Midships -----	51
21.	0° Yaw: 1.1° Pitch Up, 6° Port Roll, Stern -----	51
22.	0° Yaw: 0° Pitch, 6° Stbd Roll, Bow -----	52
23.	0° Yaw: 0° Pitch, 6° Stbd Roll, Midships -----	52

24.	0° Yaw: 0° Pitch, 6° Stbd Roll, Stern -----	53
25.	0° Yaw: 1.1° Pitch Up, 6° Stbd Roll, Bow -----	53
26.	0° Yaw: 1.1° Pitch Up, 6° Stbd Roll, Midships ----	54
27.	0° Yaw: 1.1° Pitch Up, 6° Stbd Roll, Stern -----	54
28.	45° Port Yaw: 0° Pitch, 0° Roll, Bow -----	56
29.	45° Port Yaw: 0° Pitch, 0° Roll, Midships -----	56
30.	45° Port Yaw: 0° Pitch, 0° Roll, Stern -----	57
31.	45° Port Yaw: 1.1° Pitch Up, 0° Roll, Bow -----	57
32.	45° Port Yaw: 1.1° Pitch Up, 0° Roll, Midships ---	58
33.	45° Port Yaw: 1.1° Pitch Up, 0° Roll, Stern -----	58
34.	45° Port Yaw: 0° Pitch, 6° Port Roll, Bow -----	60
35.	45° Port Yaw: 0° Pitch, 6° Port Roll, Midships ---	60
36.	45° Port Yaw: 0° Pitch, 6° Port Roll, Stern -----	61
37.	45° Port Yaw: 1.1° Pitch Up, 6° Port Roll, Bow ---	61
38.	45° Port Yaw: 1.1° Pitch Up, 6° Port Roll, Midships -----	62
39.	45° Port Yaw: 1.1° Pitch Up, 6° Port Roll, Stern -----	62
40.	45° Port Yaw: 0° Pitch, 6° Stbd Roll, Bow -----	63
41.	45° Port Yaw: 0° Pitch, 6° Stbd Roll, Midships ---	63
42.	45° Port Yaw: 0° Pitch, 6° Stbd Roll, Stern -----	64
43.	45° Port Yaw: 1.1° Pitch Up, 6° Stbd Roll, Bow ---	64
44.	45° Port Yaw: 1.1° Pitch Up, 6° Stbd Roll, Midships -----	66
45.	45° Port Yaw: 1.1° Pitch Up, 6° Stbd Roll, Stern -----	66
46.	30° Stbd Yaw: 0° Pitch, 0° Roll, Bow -----	68
47.	30° Stbd Yaw: 0° Pitch, 0° Roll, Midships -----	68

48.	30° Stbd Yaw: 0° Pitch, 0° Roll, Stern -----	69
49.	30° Stbd Yaw: 1.1° Pitch Up, 0° Roll, Bow -----	69
50.	30° Stbd Yaw: 1.1° Pitch Up, 0° Roll, Midships ---	70
51.	30° Stbd Yaw: 1.1° Pitch Up, 0° Roll, Stern -----	70
52.	30° Stbd Yaw: 0° Pitch, 6° Port Roll, Bow -----	71
53.	30° Stbd Yaw: 0° Pitch, 6° Port Roll, Midships ---	71
54.	30° Stbd Yaw: 0° Pitch, 6° Port Roll, Stern -----	72
55.	30° Stbd Yaw: 1.1° Pitch Up, 6° Port Roll, Bow ---	72
56.	30° Stbd Yaw: 1.1° Pitch Up, 6° Port Roll, Midships -----	74
57.	30° Stbd Yaw: 1.1° Pitch Up, 6° Port Roll, Stern -----	74
58.	30° Stbd Yaw: 0° Pitch, 6° Stbd Roll, Bow -----	75
59.	30° Stbd Yaw: 0° Pitch, 6° Stbd Roll, Midships ---	75
60.	30° Stbd Yaw: 0° Pitch, 6° Stbd Roll, Stern -----	76
61.	30° Stbd Yaw: 1.1° Pitch Up, 6° Stbd Roll, Bow ---	76
62.	30° Stbd Yaw: 1.1° Pitch Up, 6° Stbd Roll, Midships -----	77
63.	30° Stbd Yaw: 1.1° Pitch Up, 6° Stbd Roll, Stern -----	77

ACKNOWLEDGMENTS

Sincere appreciation is extended to Dr. J. Val Healey of the Naval Postgraduate School Department of Aeronautics and Astronautics for his guiding hand throughout this study. Thanks is extended to LCDR Tom Cahill for his lessons learned and to LCDR Mike Johns for his timely and enthusiastic wind tunnel assistance. Without the sense of urgency exhibited by LT S.R. Parker, Officer-in-Charge, Navy Resale Activity Detachment, Cubi Point, Phillipines, the scale LHA model would never have existed. Ms Dale Ward, Mr. Andy Sarakon and Mr. Mitch Nichols of the NPS Photo Lab for their responsiveness to photographic requirements, and Mr. Ron Ramaker and Mr. John Moulton, Department of Aeronautics and Astronautics technicians, were all of invaluable assistance. Thanks is extended to Mr. Bob Lande for typing the hand-scribed manuscript. My motivation for coming to Monterey and continual encouragement throughout my studies here is due solely to the support given me by my wife [REDACTED] and children, [REDACTED]--this paper is the result of that support. Finally, I am thankful to God for the many blessings given me that have enabled me to complete this work.

I. INTRODUCTION

Presently the U.S. Navy operates helicopter aviation units from combatant, auxiliary and amphibious class ships. These units perform varying missions that include anti-submarine warfare, targeting, logistics delivery, marine amphibious assault and general personnel transport. Their utility is interwoven into the fabric of the fundamental war fighting tactics of the Navy. In spite of the helicopter's focal point in fleet operations, their usage presents a significant problem in their marriage to the numerous non-traditional and small landing platforms mentioned above.

Ships, as landing platforms, introduce an unquantified airwake during helicopter rotor engage/disengage and launch/recovery operations. These airwakes, when viewed from the daily environment of ships at sea, namely high winds, turbulent seas and the resulting pitch and roll of the deck, introduce a new aspect to safe and successful operation of helicopters.

This study will take the first step towards a qualitative analysis of the airwake of a TARAWA class LHA in a simulated atmospheric boundary layer. Using the environmental wind tunnel at the Naval Postgraduate School, Monterey, California, helium bubble flow visualization techniques will be employed and a photographic record of the resulting

airwakes will be presented. The ultimate goal of this analysis, under the direction of Dr. J.V. Healey, is the quantification of the turbulence levels in the airwake with an eye towards a determination of safe operating envelopes for helicopters by computer simulation. This thesis, however, will merely qualitatively map one such airwake.

As mentioned above, the center of attraction is the TARAWA class LHA. This class of ship is the major player in the U.S. Navy's amphibious assault operations. A large ship (length: 820 ft, beam: 106 ft, draft: 26 ft, displacement: 39,300 tons), the LHA combines the features of floodable well deck operations previously employed in LSD and LPD class ships, and helicopter assault as seen in LPH class ships. This study utilizes a 1:205 scale wooden model of the LHA, suitably mounted to a motion simulator able to fix various combinations of pitch, roll and yaw.

The flow via helium bubble flow visualization will be photographed, at each of the pitch and roll combinations selected for several yaw angles, and discussed in detail. Additionally a brief review of the salient features of the atmospheric boundary layer, ship motion analysis and helium bubble flow visualization technique will be presented. Past modifications to the NPS environmental wind tunnel will be discussed for continuity purposes.

II. ATMOSPHERIC BOUNDARY LAYER MODELING

A. THEORY

Fundamental to the airwake study of any hull form is the proper modeling of the atmospheric boundary layer (ABL). The ABL can be viewed as a turbulent layer which is primarily a function of friction, roughness height, thermal layers and Coriolis forces. In [Ref. 1], Arya defines the lowest 100 meters of the ABL as the surface layer. Distinguished by sharp fluctuations in wind speed and temperature, the surface layer is noted by turbulence born of surface roughness or friction. This turbulence is the primary cause of the vertical exchanges of momentum to and from the surface. As noted by Arya, several simplifying features have been discovered concerning the surface layer. Vertical momentum flux and wind direction remain nearly constant with height while the flow structure is not significantly affected by Coriolis acceleration.

Two factors of primary importance that affect the ABL are gradient winds and surface roughness. This study will assume that gradient winds are constant with height. Since the ABL is propelled by large-scale atmospheric flows, among them gradient winds, and that variations in these flows are insignificant over the largest horizontal scale of this study, this assumption can be readily accepted. Surface roughness has been found to be a primary factor influencing

surface drag. As stated in Arya, surface drag is principally responsible for the characteristic wind profile in the surface layer of the ABL. The resulting wind shear creates much of the turbulence in the surface layer. Therefore, it can be seen that surface roughness plays an integral part in the mean velocity profile and turbulence structure of the surface layer in the ABL.

In the neutral density ABL near the surface the constant momentum flux noted earlier leads to the well-known logarithmic wind profile,

$$\frac{\bar{U}}{U_*} = \frac{1}{k} \ln \frac{z}{z_0} \quad (1)$$

where \bar{U} is the average velocity, U_* is the friction velocity, z_0 is the roughness parameter, z the vertical distance from the surface, and k is von Karman's constant. An alternative version of Equation (1) given by Davenport in [Ref. 2], yields the expression,

$$\frac{\bar{U}}{U_g} = \left(\frac{z}{z_g} \right)^n \quad (2)$$

This is the Power Law Velocity Profile, where U_g is the gradient velocity and z_g the gradient height. The exponent n is a scaling parameter to be more fully developed during the ensuing discussion on wind tunnel modeling of the ABL. It is this Power Law Velocity Profile that was used to model

the ABL in the environmental wind tunnel at the Naval Postgraduate School.

B. WIND TUNNEL MODELING

As noted by Healey in [Ref. 3], the flow field is substantially altered by the presence of wind shear and turbulence in the free-stream flow. Additionally he notes that it is insufficient to merely model the mean velocity profile when simulating the ABL in an environmental wind tunnel. With this in mind there are four parameters of significance to the free-stream airflow as it impinges on a given hull form:

1. The windspeed averaged over a period of time, somewhere between ten minutes and an hour, called the mean speed.
2. The standard deviation, σ , of the longitudinal (along wind) wind speed fluctuations about the mean which, when divided by the mean speed is defined as the turbulence intensity.
3. The longitudinal length scale of the turbulence, L , or "integral" length scale, which is a measure of the size of the strongest eddies in the turbulence.
4. The turbulence spectrum function defined as the energy distribution of the frequencies present in the turbulence.

Empirical relationships, E.S.D.U. data items 74030 and 74031 [Ref. 4], describe the above four parameters as a function of:

1. The mean wind speed, $U(Z)$, measured in meters/sec, a function of elevation.
2. The elevation, Z , measured in meters, above the mean obstruction height of a surface which in this study is the mean wave height in sea water.

3. The roughness length scale, z_0 , measured in meters, a measure of surface roughness, containing no direct relationships to the height of sea obstacles, waves. Davenport [Ref. 2], states that values of z_0 for the sea surface range from .001 to .01 meters.

Figures 1 through 3, from E.S.D.U. 74031, can be used to estimate the surface roughness parameter, z_0 , the turbulence intensity, σ/U , and the length scale parameter, L .

Based on the particular model chosen (an LHA for this study), a specific elevation Z can be chosen which is defined as the height of the flight deck above the mean sea surface. Additionally a mean wind speed, $U(Z)$, can be chosen. These two independent variables are used to determine the roughness length scale, z_0 , as developed by Garratt in [Ref. 5]. By use of the relationships between the drag coefficient for the neutral airflow over the sea and the mean wind speed:

$$C_d = [0.75 + 0.067U(Z)] \times 10^{-3} \quad (3)$$

and the Monin-Obukov similarity theory

$$k / \sqrt{C_{d_n}} = -\ln(Z/z_0) \quad (4)$$

where k , the von Karman constant, is approximately 0.41, C_{d_n} may be eliminated from Equations (3) and (4) yielding the expression:

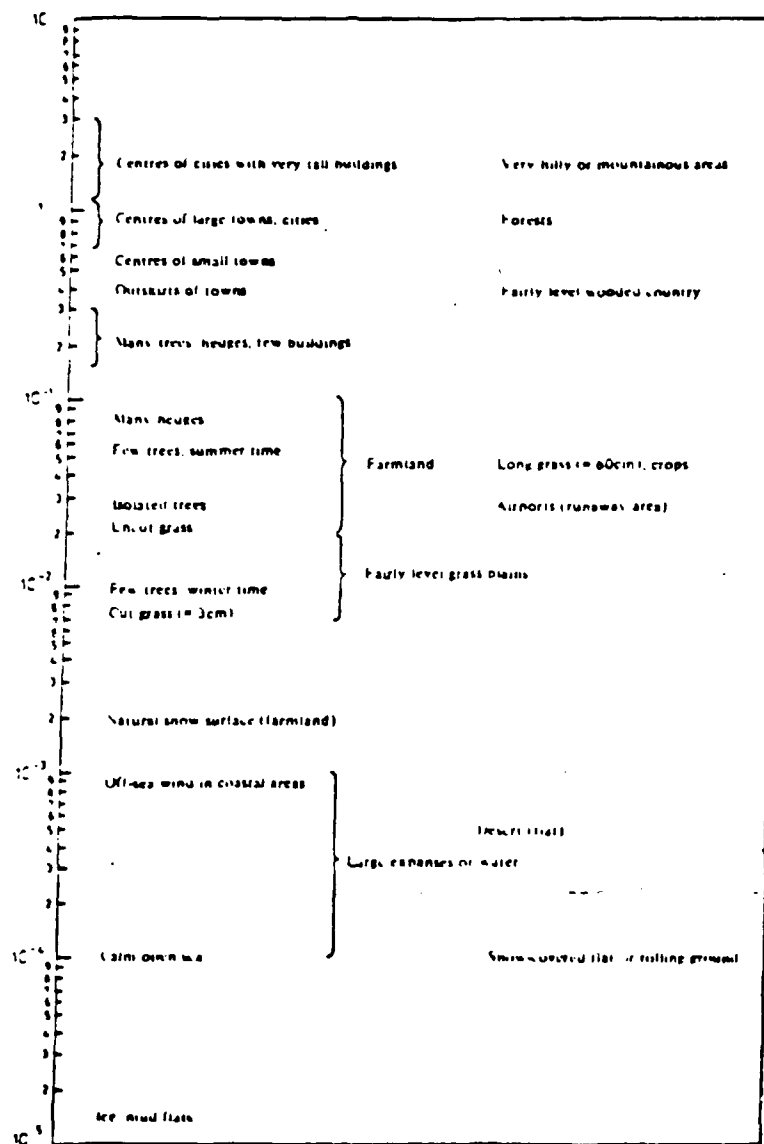


Figure 1. Surface Roughness Parameter z_0 (from ESDU 74031)

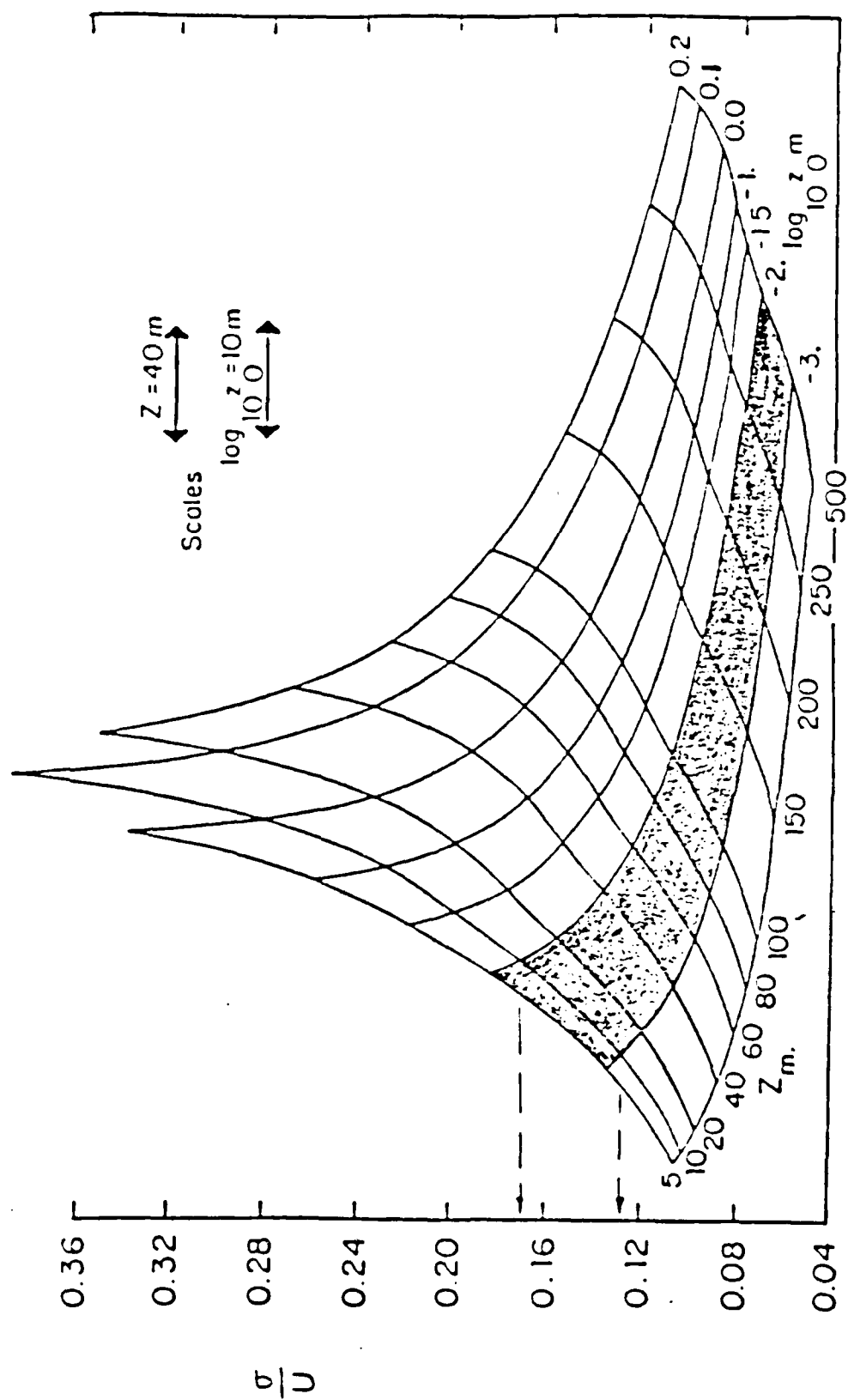


Figure 2. The (Longitudinal) Turbulence Intensity (from ESDU)

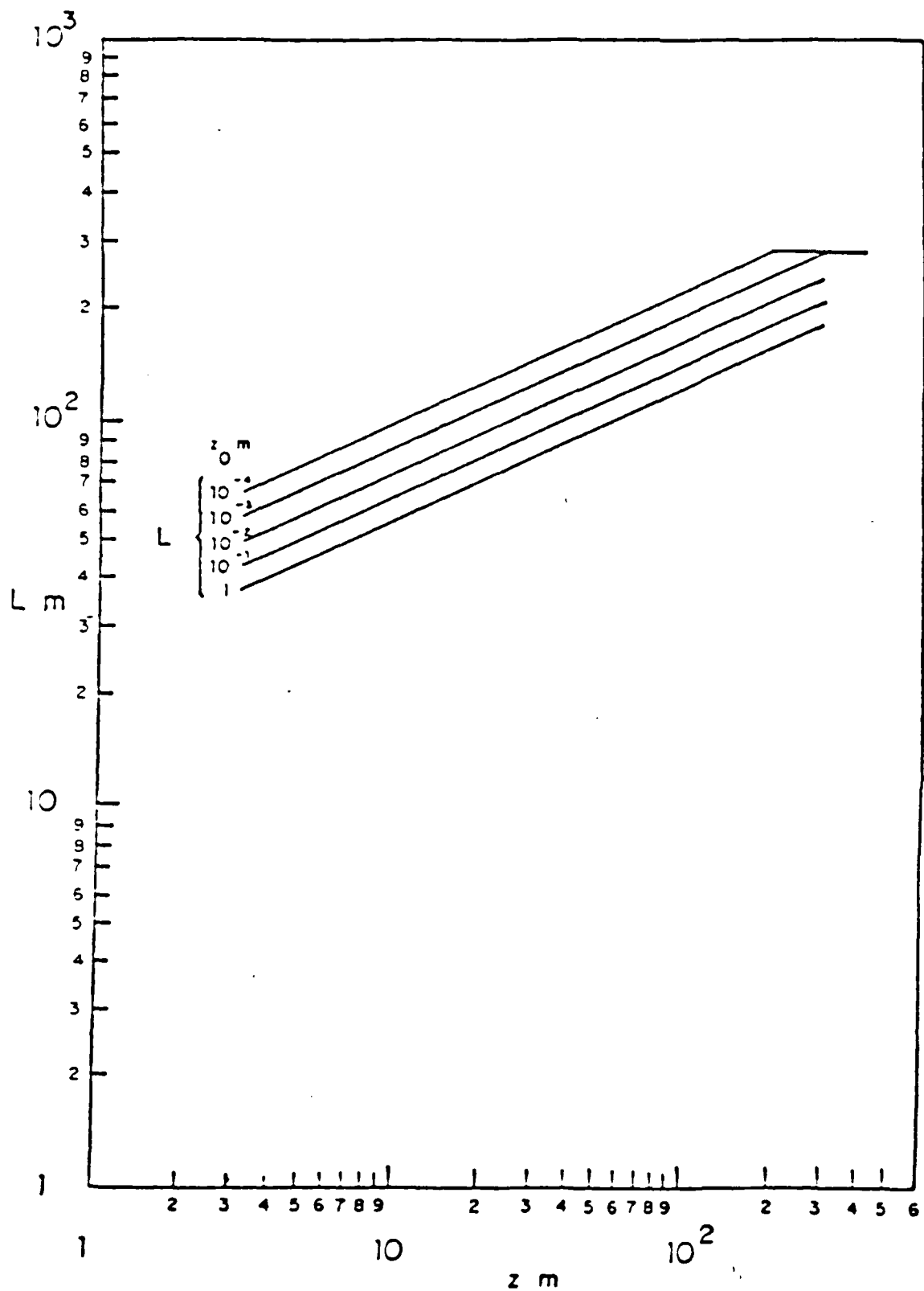


Figure 3. Values of the Length Scale Parameter L (from ESDU)

$$z_0 = Z \exp\{-0.41/[(0.067U(Z) + 0.75) \cdot 10^{-3}]^{1/2}\} \quad (5)$$

Now, as Z and z_0 are both known, Figure 2 may be entered in order to determine the turbulence intensity level, $\%U$.

In [Ref. 3], Healey notes that the length scale, L , is not in and of itself very important, but rather the ratio of the length scale to the characteristic body dimension of the ship. (This study will use the beam of the ship.) The length scale can be obtained from Figure 3.

The Power Law Velocity Profile, previously stated as Equation (2), has a distinct advantage in modeling the ABL in that it has only one scaling, or shape, parameter, namely the exponent n . In data collected by Counihan [Ref. 6], evidence indicates that for natural surfaces there exists a one to one correspondence between this exponent and the surface roughness. Furthermore, Plate in [Ref. 7] states that in a wind tunnel any exponent n can be determined by a suitable arrangement of roughness elements and externally impressed disturbances such as grids or fences at the inlet of the test section. Implied in his work is that, given a proper value of n for the Power Law Velocity Profile equation, the resulting wind profile, wind shear and turbulence intensity of the ABL can be properly modeled in an environmental wind tunnel. Indeed Plate states that the turbulent boundary layers which are the analog of the idealized ABL are essentially equilibrium layers, in that if

the exponent n and the turbulence profiles are the same, then the mean flow quantities are similar for both the prototype and model.

Central to the issue of modeling the turbulent ABL is how to do so in a short test section. This is done, as previously suggested, by the use of an appropriate array of trip fences and roughness elements. As indicated by Plate, profiles immediately downstream of any triggering device are not of the equilibrium type. However, experiments, most notably those of Counihan in [Ref. 6], involving the use of boundary layer tripping devices such as sharp-edged castellated or saw-tooth-shaped fences and roughness elements on the tunnel floor, achieve the desired result of matching the exponent n of the turbulence. These devices have the effect of creating an initially thick boundary layer, that further downstream develops into an equilibrium boundary layer which is adjusted to the uniform roughness of the tunnel floor.

Using the techniques of Counihan, the environmental wind tunnel at the Naval Postgraduate School was modified to correctly model the turbulent ABL. An overview of this procedure will be discussed in Chapter IV which deals with experimental apparatus. It is appropriate at this point to state the observation of Healey in [Ref. 3]. Many of the wind tunnels that simulate the earth's atmosphere have done so with an eye towards self-excited oscillations of

buildings and bridges. Their tendency was to concentrate on pressure distributions and how they cause structure movement. Details of the flowfield were not of primary importance. This study, however, will concentrate on the flowfield itself and how it ultimately impacts the helicopter/ship interface.

III. SHIP MOTION

A. THEORY

Ship motion analysis can be viewed as a vibrating body. The mathematical model of this motion is that of a set of six springs, masses and dampers for a six degree of freedom system and is expressed as:

$$MY''(t) + DY'(t) + KY(t) = F(t) \quad (6)$$

where M, D and K are 6 x 6 matrices and Y and F are 6 dimensional vectors. Each displacement requires a coordinate to describe it, therefore this model is composed of the coordinates (x,y,z,φ,θ,ψ), three are translational--heave, sway and surge (z,y,x), and three are rotational--roll, pitch, and yaw (φ,θ,ψ).

In [Ref. 3] Healey discusses the components of Equation (6). F represents a six-component vector, composed of three forces and three moments, and results from irregular sea motion in the vicinity of the ship. Y is the vector (x,y,z,φ,θ,ψ).

A natural consequence of the motion of the water surrounding any ship is that some of its motion components are in phase with that of the ship. In this regard these components are additive, thereby giving the ship "added"

masses and inertias. M therefore represents the "virtual" mass matrix, the components of which are the sums of the ship mass and inertias and the added mass and inertias.

Matrix K , representing the hydrostatic restoring force, can be calculated based on the known hull geometry of any ship.

Finally, the damping matrix D , is composed of:

1. External viscous term arising from skin friction on the hull, keel, rudder, fins, etc.
2. Internal viscous terms derived from bilge keel water motion.
3. Dynamic lift which creates speed dependent terms.
4. Wave and eddy making ship activities.

Using "strip theory" approximation, coefficients and forces, as they relate to Equation (5), are computed. Strip theory allows calculation of the added terms in the mass matrix, the inviscid contributions to the damping coefficient and the forces and moment on the hull. Empirical or semi-empirical results govern the remaining terms of the damping matrix discussed above.

It is appropriate at this point to discuss briefly what it is that causes ship motion, namely sea motion. Healey [Ref. 3] describes the energy in waves as nearly a log-normal distribution, in that waves contain little energy at very low frequencies while the energy rises steeply with increasing frequency to a maximum and then tapers off slowly. Waves may be classified as either long crested or

short crested. Long crested waves have as their origin far away storm centers. These waves propagate with long crests forming parallel lines. Large amplitude ship motions are the result of such waves. On the other hand, short crested waves have no consensus as to their direction or front and may be thought of as confused seas. These are born of local winds and are of primary interest to the ship/sea interface problem in that they produce both pitch and roll motions regardless of ship heading. Long crested waves, however, produce no roll response in head seas and no pitch response in beam seas.

The energy transfer from wind to the sea takes up to 24 hours for a fully developed sea. The sea wave spectrum function can be described by many useful models, one of which will be discussed in the following section that deals with ship motion prediction methods. However the spectrum that the ship experiences will vary from the wave function. The ship's "encounter frequency," according to Healey, will depend on the heading, the angle between the ship direction and the dominant wave direction.

This then leads us to how to compute the displacements as described by Equation (5). As summarized by Biskaduros [Ref. 8], there are two primary methods of ship motion calculation--time domain and frequency analysis. The time domain approach approximates the coefficient matrices, uncoupling the roll motion by simple coordinate

transformations. This approach is valid only for small movement of the ship about its equilibrium state and its accuracy falls off as the amplitudes of motions increase. The frequency analysis method ratios the wave encounter frequency to the ship response of any particular degree of freedom. This ratio, called the Response Amplitude Operator (RAO), is a function of wave frequency, ship's heading and speed, sea condition and each degree of freedom. Although easily calculated, the sheer number of RAO's required necessitates use of computer-oriented computational methods. David Taylor Naval Ship Research and Development Center (DTNSRDC) has developed computer software, which is a sophisticated predictive tool, a description of which will be discussed next.

B. SHIP MOTION PROGRAM SOFTWARE

The Standard Ship Motion Computer Program (SMP) was developed by DTNSRDC as a method of predicting ship motion. The SMP users manual [Ref. 9] describes in detail the theory, as well as the lines of coding that make up the SMP. For continuity purposes, a brief synopsis will be presented in this paper.

SMP provides both a revision and compilation of several programs previously used for some portion of the ship/sea motion prediction. A previous ship motion program used by DTNSRDC called Sea Motion and Sea Load Computer Program (SMSL) provided ship motion and load predictions in six

degrees of freedom for any ship at a constant speed and arbitrary heading in regular waves. To cover the aspect of irregular waves, ESPEC was developed to provide Root Mean Square (RMS) motion values in both long and short crested waves. These seas were modeled using a two parameter Bretschneider wave spectrum representation, with the two parameters being significant wave height and modal wave period. Finally, as SMP was being written, DTNSRDC contracted and had written a program called SHREDS. Used in conjunction with SMSL, SHREDS provided irregular sea predictions. SMP therefore combines SMSL, ESPEC and SHREDS in order to provide predictive ship motion data in both regular and irregular seas.

These predictions cover both translational and angular ship statistical responses, and are based on the product of a ship's response amplitude operator (RAO), sea spectra and the frequency mapping. As noted by Healey [Ref. 3], the comparison of model tests and the predictions of SMP show good agreement. Pitch prediction is very good while other motions showed inconsistent results. However, as noted in an update to SMP [Ref. 10], errors occurred in bilge keel calculations and upon correction SMP exhibited improved roll predictions.

C. EXPERIMENTAL MODELING

In attempting to model ship motion in the ABL a match between the motion of a full scale ship and that of a scaled

model must occur. At this point in the discussion, the Strouhal number is introduced.

$$\text{Strouhal Number} = nb/U \quad (7)$$

where n is the inverse of the sea encounter period or the frequency of oscillation, b is the characteristic length (for the purpose of this study, this equates to the beam of the ship), and U is the wind speed. Therefore in order to accurately model the motion of any ship, Strouhal numbers must be equated.

First consider the full scale LHA, the ship under discussion in this airwake study. Values for n , in both pitch and roll, were provided by Mr. Eric Baitis of DTNSRDC from SMP calculated data; n (pitch) = 1.12° , 0.125 Hz, n (roll) = 6° , 0.067 Hz. b , the ship's beam is 32.31 meters. In addressing wind speed it is advantageous to analyze the worst case situation for an airwake, in other words, the maximum wind conditions for the ship in question. To determine this, Equation (5), reprinted below, will be used.

$$z_0 = Z \exp\{-0.41/[(0.067U(Z) + 0.75) 10^{-3}]^{1/2}\} \quad (5)$$

Z , the height of the flight deck above the sea surface is 19.66 meters for an LHA. z_0 is determined from E.S.D.U. previously reprinted as Figure 2 in Chapter II. Entering

arguments for Figure 2 are Z and σ/U , the turbulence intensity. Modifications to the Naval Postgraduate School environmental wind tunnel, in order to correctly model the ABL, were performed by Bolinger, as reported in [Ref. 11]. (Details of this modification will be discussed in Chapter III which describes the experimental apparatus.) Based on this modification, the lower four inches of the wind tunnel, that portion the LHA model will occupy, shows an average turbulence intensity of 0.1157. Entering Table 2 with these values produces a z_0 of 0.000794, slightly outside the range of 0.001 to 0.01 as reported by Davenport [Ref. 2], and previously mentioned in Chapter II. Now, solving Equation (5) yields a $U(Z)$ of 13.318 meters/second, or 25.87 knots of wind speed. This wind speed corresponds to sea state 5, 8-13 foot seas, as tabulated in Bowditch [Ref. 12].

Next consider the scaled LHA model. b , the ship's beam is 0.157 meters. Again, looking at the lower eight inches of the wind tunnel, Bolinger [Ref. 11], reports an average wind speed of 2.02 meters/second. Now, using Equation (7) and equating Strouhal numbers of both the full scale and scaled model of the LHA, values for n , in both pitch and roll, are calculated to be: n (pitch) = 1.12° , 3.902 Hz, n (roll) = 6° , 2.091 Hz.

The data expressed above are tabulated below.

TABLE 1
SHIP MOTION PARAMETERS

<u>Variable</u>	<u>Ship</u>	<u>Model</u>
b (beam)	32.31 meters	0.157 meters
U (velocity)	15.67 meters/sec	1.96 meters/sec
n (pitch)	1.12°, 0.125 Hz	1.12°, 3.902 Hz
n (roll)	6°, 0.0667 Hz	6°, 2.091 Hz

D. BLUFF BODY AERODYNAMICS

Healey [Ref. 3] describes the characteristics of a bluff body as those exhibiting massive separated wakes. At sufficiently high Reynolds number, examples are provided by cylinders or prisms or airfoils at high angle of attack. This wake is usually accompanied by a complex vortex system that may be stationary or periodically shedding. Shedding appears to be a 2-D phenomenon. Furthermore the flow field near such bodies is substantially altered by the presence of shear and turbulence in the free-stream flow.

Because the long-term aim is to replace current interface testing with simulation, the need to study the ship airwake is of paramount importance to the U.S. Navy. The ship itself is a bluff body, or a cluster of bluff bodies, hence the need for this relatively obscure branch of aerodynamics. As noted by Biskaduros [Ref. 8], two areas of interest with oscillating bluff bodies are trailing vortices and flow detachment and reattachment. A determination for any given ship, of the strengths of trailing vortices and

their height above the deck, those areas where flow detachment and reattachment is observed, and how this is affected by motion of that ship, would greatly aid the operation and control of helicopters from the decks of U.S. navy ships. This study, and how it applies to an LHA class ship, is an attempt at gaining just such an insight.

IV. EXPERIMENTAL APPARATUS

A. WIND TUNNEL DESCRIPTION

The environmental wind tunnel at the Naval Postgraduate School (NPS), Monterey, California was used during the course of this study. As depicted in Figure 4, the tunnel is a modified three-dimensional open circuit smoke tunnel. Modifications will be discussed in the next section. Air flow is through three inches of honeycomb and a mesh screen into a square bell contraction cone with a contraction ration of 9:1. The inlet measures 15 x 15 feet and is contracted to a test section of 5 x 5 feet that is 22 feet long.

Immediately aft of the test section louvers are in place in order to close off flow when the tunnel is secured thereby preventing autorotation of the tunnel fan. Aft of the louvers, the tunnel transitions to a circular duct. Contained in the circular duct is a variable pitch fan used to control the tunnel wind speed. Lastly, the air flow direction is changed 90 degrees by turning vanes and exhausted upward to the atmosphere.

The tunnel (roof and sides) are fitted with plexiglass and plateglass windows used for a variety of purposes to include viewing, lighting and photography. The viewing window allows photography to within four inches of the

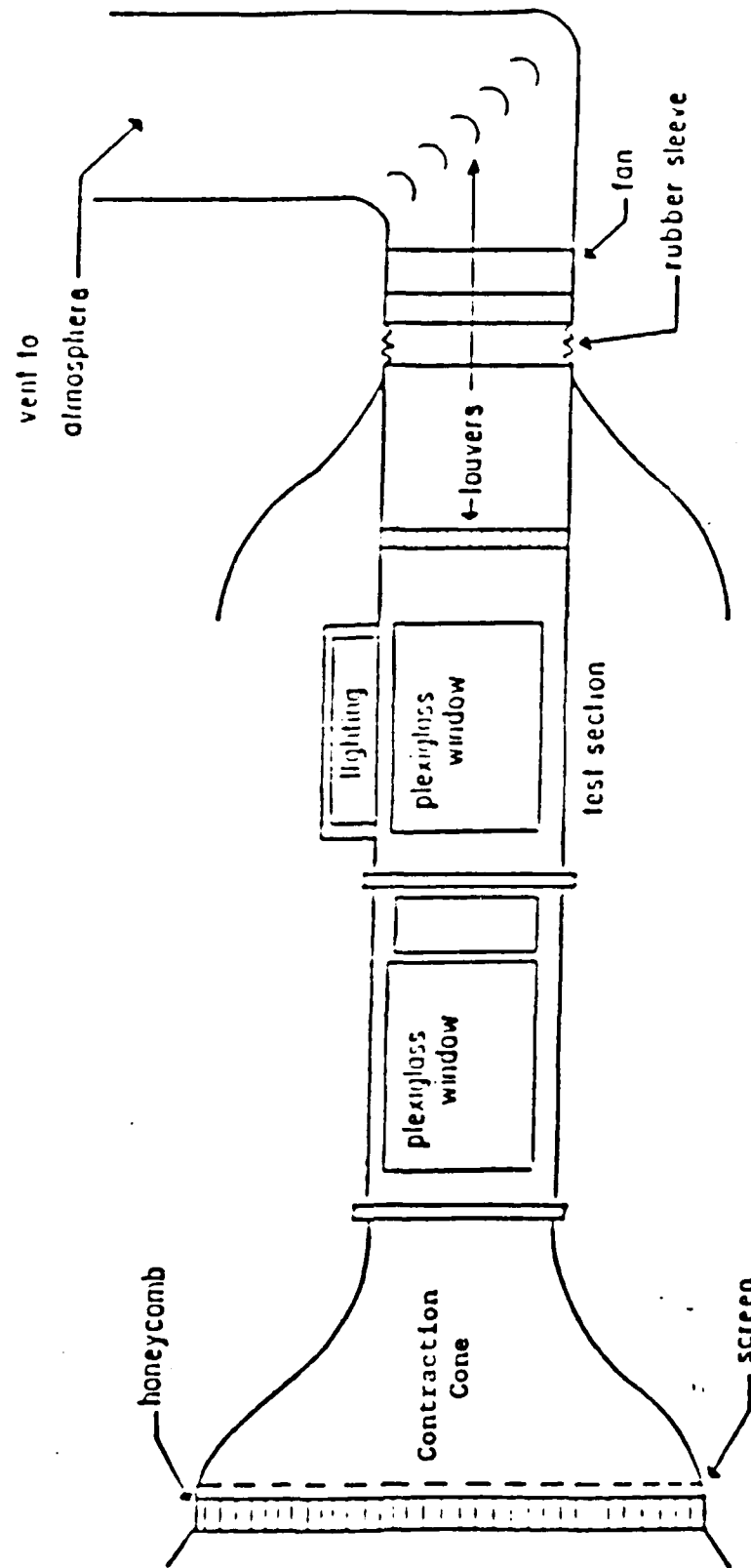
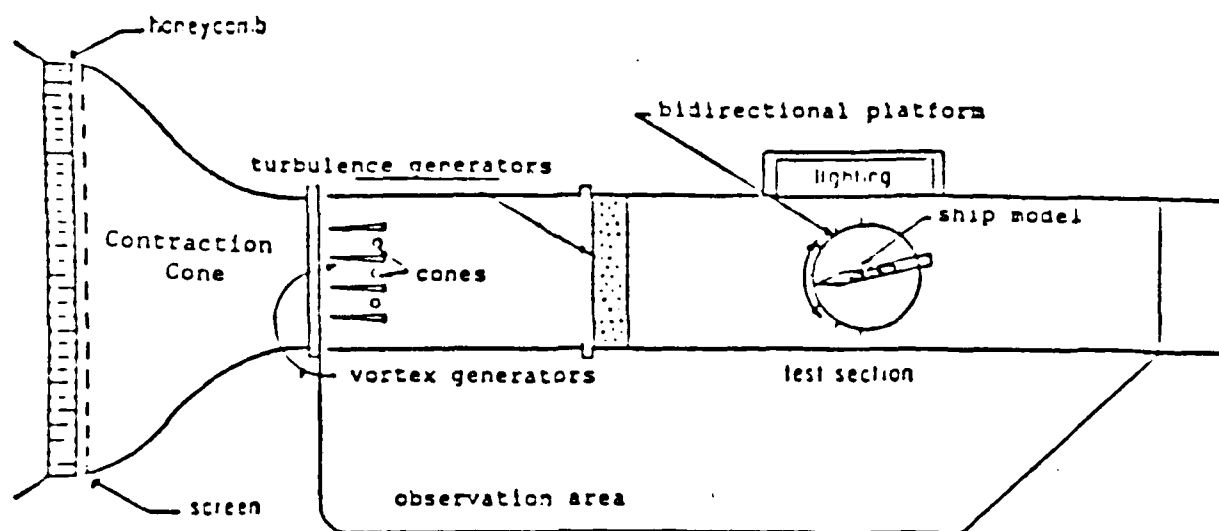


Figure 4. Schematic of the Naval Postgraduate School Flow Visualization Tunnel [Bolinger, Ref. 11]

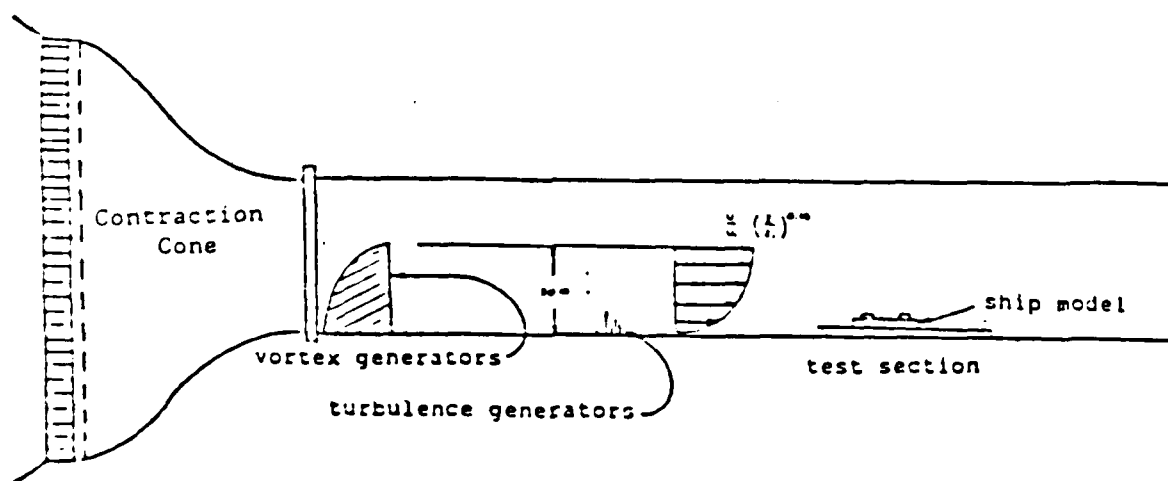
tunnel floor and approximately 12 inches aft of the model placement area. This allows greater flexibility in photographing the airwakes of ships, especially those aft of the helodeck, a predominant approach area for cruiser and destroyer type aviation capable platforms. The tunnel has a 51 inch diameter circular platform cut into the floor for mounting of ship models. Inside this circular area is a 15 x 51 inch rectangle centered on the circle origin that can be changed to fit various sizes of models. In this way the overall circular platform remains while being only slightly modified to accept different size ship models. Finally, the tunnel interior is painted flat black so as to minimize light reflection during flow visualization photography.

B. WIND TUNNEL MODIFICATIONS

As was previously discussed in Chapter II, Bolinger, in [Ref. 11], modified the environmental wind tunnel at NPS based on the work of Counihan as stated in [Ref. 6]. Prior to any changes to the NPS tunnel, the velocity profile was nearly uniform and the turbulence level was less than one percent, hardly a close approximation to the ABL. As sketched in Figure 5, four vortex generators and three tapered two inch diameter cones, interspaced between the vortex generators, all of which were 30 inches high, were placed immediately aft of the contraction cone. The resulting velocity profile was found to match the Power Law



Plan View



Elevation

Figure 5. NPS Flow Visualization Tunnel
[Bolinger, Ref. 11]

Velocity Profile expression, previously stated in Chapter II and repeated here for continuity:

$$\frac{\bar{U}}{U_g} = \left(\frac{z}{z_g}\right)^n \quad (2)$$

Additionally, the distribution was horizontally uniform as is the case in the true ABL. The value of the exponent n was determined to be 0.139, within the range of 0.11-0.15 as indicated by Davenport in [Ref. 2]. Having attained this match, the turbulence level was pursued. By placing various lengths of 3/8 inch dowels, ranging from one to six inches long, in a random fashion over an 18 inch x 5 foot section of the tunnel floor upstream of the model placement area, a turbulence intensity level of approximately 12 percent was attained.

Measurements of the velocity profile were accomplished using a DANTEC hot wire anemometer, calibrated with an EDM 2500C micromanometer, to a test section height of 30 inches. Results are as shown in Table 2, reprinted from Bolinger [Ref. 11]. Likewise turbulence intensity levels are reprinted from Bolinger and shown as Table 3. As was discussed in Chapter III, our primary interest lies in the lower four inches of the ABL where the average turbulence intensity is approximately 12 percent and the mean velocity is 2.02 meters/sec.

TABLE 2

TEST SECTION VELOCITY DATA (ft/sec)

x'	Z- Height above floor (inches)								
	2.00	3.00	4.00	8.00	12.00	16.00	19.00	25.00	30.00
6.00	6.21	6.36	6.63	7.81	7.84	8.13	8.44	8.61	9.15
9.00	6.32	6.35	6.84	7.89	7.78	8.00	8.40	8.60	9.23
12.00	6.24	6.40	6.88	7.83	7.80	8.09	8.37	8.65	9.16
15.00	6.29	6.39	6.78	7.65	7.88	8.25	8.40	8.65	9.21
18.00	6.23	6.41	6.58	7.53	7.90	8.17	8.41	8.43	9.07
21.00	6.34	6.43	6.70	7.80	8.05	8.16	8.53	8.59	9.27
24.00	6.30	6.13	6.74	7.79	8.01	8.09	8.49	8.51	9.24
27.00	6.28	6.26	6.85	7.77	7.96	8.05	8.41	8.60	9.01
30.00	6.24	6.22	6.77	7.85	7.89	8.01	8.28	8.58	9.21
33.00	6.22	6.30	6.65	7.79	7.84	7.98	8.38	8.56	8.96
36.00	6.31	6.10	6.71	7.56	7.78	8.06	8.43	8.64	8.91
39.00	6.29	6.17	6.74	7.66	7.80	8.09	8.44	8.59	9.21
42.00	6.26	6.20	6.72	7.76	7.82	8.07	8.34	8.57	8.98
45.00	6.33	6.37	6.83	7.76	7.85	8.06	8.34	8.63	9.03
48.00	6.25	6.34	6.73	7.84	7.95	8.27	8.38	8.64	8.83
51.00	6.25	6.27	6.79	7.77	8.01	8.24	8.44	8.77	9.08
AVE.	6.27	6.29	6.75	7.75	7.89	8.11	8.41	8.60	9.10
V/Vo	0.68	0.69	0.74	0.85	0.87	0.89	0.92	0.95	1.00
SIGMA	0.04	0.09	0.08	0.09	0.08	0.08	0.06	0.07	0.13

Vo at 30 inches = 9.1 ft/sec

* transverse position from far wall in inches

TABLE 3

TEST SECTION % TURBULENCE INTENSITY DATA

	Z- Height above floor (inches)								
x ⁺	2.00	3.00	4.00	8.00	12.00	16.00	19.00	25.00	30.00
6.00	11.57	12.22	13.73	3.80	3.90	3.80	3.00	3.10	1.90
9.00	11.34	11.21	11.80	3.81	3.80	3.40	2.80	2.90	1.20
12.00	12.39	13.70	11.67	3.73	3.60	3.70	3.20	2.90	1.60
15.00	12.83	12.79	10.05	4.09	3.70	3.60	3.10	3.30	1.80
18.00	12.25	13.41	11.34	4.06	4.20	4.20	3.30	4.10	3.00
21.00	11.00	13.83	8.90	5.20	3.80	3.80	3.60	2.90	2.11
24.00	11.27	12.70	12.78	6.07	4.00	3.80	3.50	3.70	1.80
27.00	11.21	10.84	10.16	5.59	3.80	3.60	3.50	3.10	2.40
30.00	11.68	12.72	11.71	4.53	3.77	3.40	2.90	2.80	1.90
33.00	11.77	11.03	11.07	5.05	3.90	3.60	2.70	2.80	2.50
36.00	11.41	11.58	9.38	6.21	4.30	3.60	3.20	3.30	2.70
39.00	12.26	11.33	9.58	5.55	4.50	3.90	3.40	3.60	2.30
42.00	12.74	12.09	12.75	4.70	3.80	3.67	3.30	3.40	2.80
45.00	12.09	12.11	10.96	4.80	3.90	3.50	3.60	3.20	2.50
48.00	12.47	12.76	12.48	4.70	3.80	3.60	2.90	2.70	2.40
53.00	11.26	12.67	12.98	4.80	4.00	3.50	3.90	3.10	2.20
=====									
AVE.	11.85	12.32	11.33	4.79	3.92	3.66	3.24	3.18	2.19
SIGMA	0.56	0.90	1.37	0.76	0.22	0.19	0.33	0.37	0.47
=====									

Vo at 30 inches = 9.1 ft/sec

* transverse position from far wall in inches

C. OSCILLATING MECHANISM

A mechanism designed for pitch and/or heave and roll was installed in the NPS environmental wind tunnel by Biskaduros [Ref. 8]. A summary of his work is presented here. The mechanism, shown in Figure 6, is mounted on a platform, trainable through 360 degrees, and located beneath the circular cutout in the tunnel floor.

Pitch motion is accomplished by means of a motor driven belt drive which turns a shaft. The motor is manufactured by Minaric Electric Company and is rated at 90V (DC), 5 amp, 1/2 hp. At either end of the shaft, a flange is fixed in place and supported by a lubricated bearing housing. An eccentric pin is located on the flanges and the pin is adjustable along the radius of the flange. The pins, in turn, ride in the slot of a "scotch yoke" to produce one stroke of vertical motion for every rotation of the flange. The yoke is aligned in a vertical orientation by teflon guides. Finally the model is fixed, forward and aft, to the top of the yokes. Heave motion, or a combination of pitch and heave, may be accomplished by 90 degree incremental rotation of both flanges after breaking a coupled flange connection on the shaft. The shaft is supported, in the vicinity of the coupled flange, by an additional lubricated bearing housing.

Roll motion is more simplified. A flange, again with an adjustable eccentric pin, is coupled directly to the roll

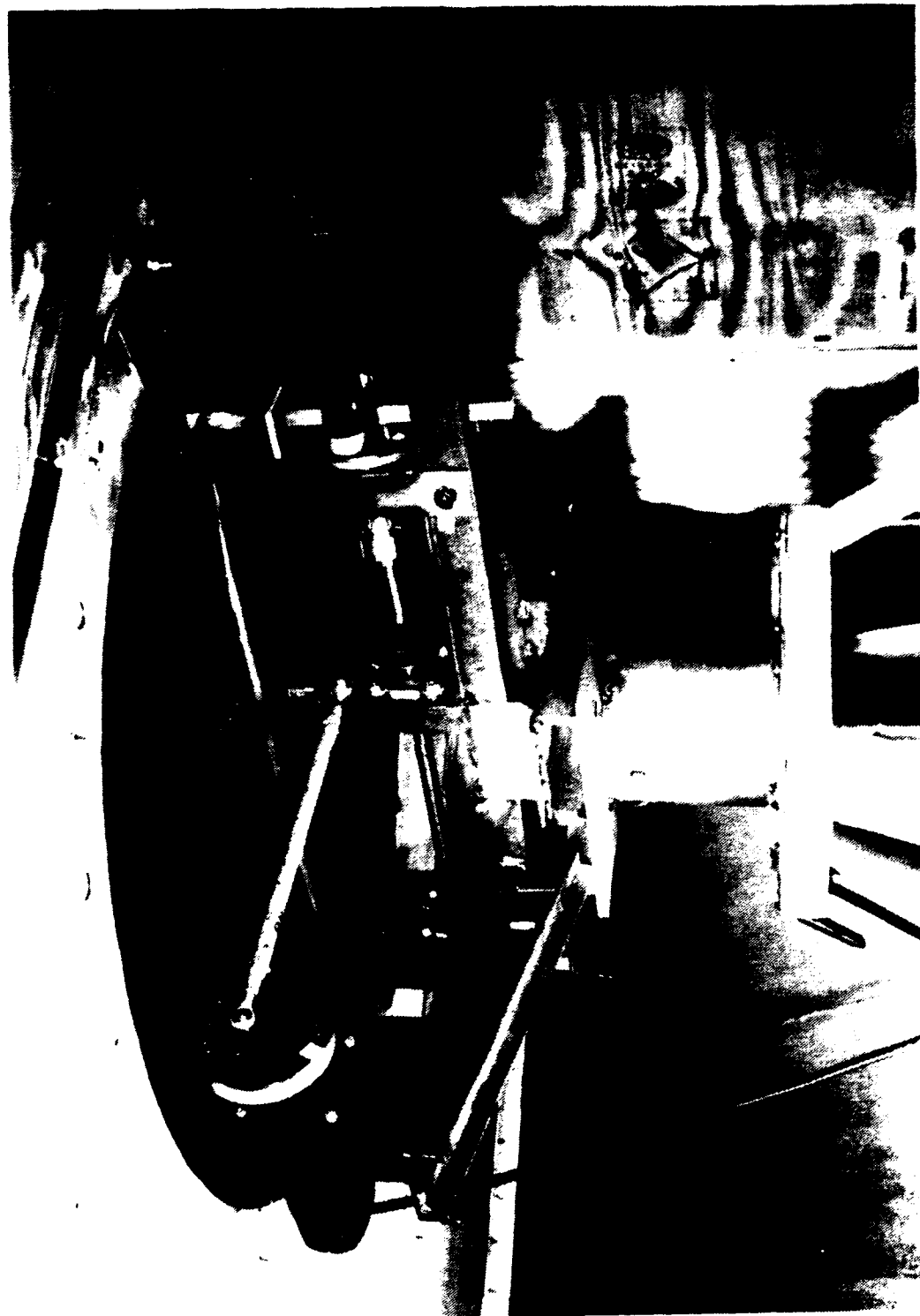


Figure 6. Ship Model Oscillating Mechanism

motor, which is rated at 130 V (DC), 1 amp, 1/8 hp and manufactured by Bodine Electric Company. A shaft fixed to the eccentric pin is pinned on the opposite end to the keel of the ship model.

In both cases, adjustment of the eccentric pin along the radius of the flange is the means by which the pitch and roll data, mentioned in Table 1 of Chapter III, is reproduced. Control boxes for both electric motors are mounted outside and to the right of the observation window of the wind tunnel.

D. SHIP MODEL

The ship model chosen for this study was a 1:205 scale model of the TARAWA Class LHA shown in Figure 7. The following prints were obtained from Mr. Erol Lewis of the Norfolk Naval Shipyard through the assistance of Mr. Roy Fuszell and Mr. Bobby Hampton of the Supervisor of Shipbuilding, Pascagoula, Mississippi: Lines and Offsets, 4521834; General Arrangement Outboard Profiles and Topside Views, 4522346. Based on these prints a scaled wooden model was produced by a vendor in the Philippines as coordinated by LT S.R. Parker, Officer in Charge, Navy Resale Activity Detachment, Cubi Point. The model was painted flat black in order to reduce reflective light during flow visualization photography. Mounting brackets were fitted to the model hull in order to fix the model in the proper orientation on the oscillating mechanism with the design water line even



Figure 7. TARAWA Class LHA

with the tunnel floor. Weather stripping was placed around the hull cut-out in the circular tunnel enclosure in order to provide an adequate seal against an influx of air from around the hull during tunnel operation. Pertinent model dimensions are summarized below:

TABLE 4

TARAWA CLASS LHA
1:205 SCALE MODEL

Length: 47.5 inches

Beam: 6.2 inches

Flight Deck Height Above Design Water Line: 3.75 Inches

V. HELIUM BUBBLE FLOW VISUALIZATION

A. BACKGROUND

This study used helium bubble flow visualization as the procedure for the qualitative analysis of the airwake around a scaled model of a TARAWA class LHA. Fundamentally the object was the use of neutrally buoyant helium bubbles to define the model's mean streamlines. Usage of helium is preferred over other methods, such as smoke, in that these bubbles will not disperse as rapidly. Secondly, since dispersion can be minimized, the bubbles, of about 1/8-inch diameter, can therefore be photographed using time exposure to trace the airwake of a given body, in this case a ship model. While the generation of helium bubbles was an easy task, lighting and photography was a more involved and iterative process. Bubble generation, lighting and photography are discussed in the following sections.

B. HELIUM BUBBLE GENERATION

Helium bubble generation was accomplished using a system manufactured by Sage Action Inc. The system, depicted in Figure 8, consists of a bubble generator console, high speed head and a vortex filter chamber. The console is externally fed by helium gas and compressed air. Internal to the console a 5 oz cylinder, used to hold bubble film solution, is located. These three components are controlled by

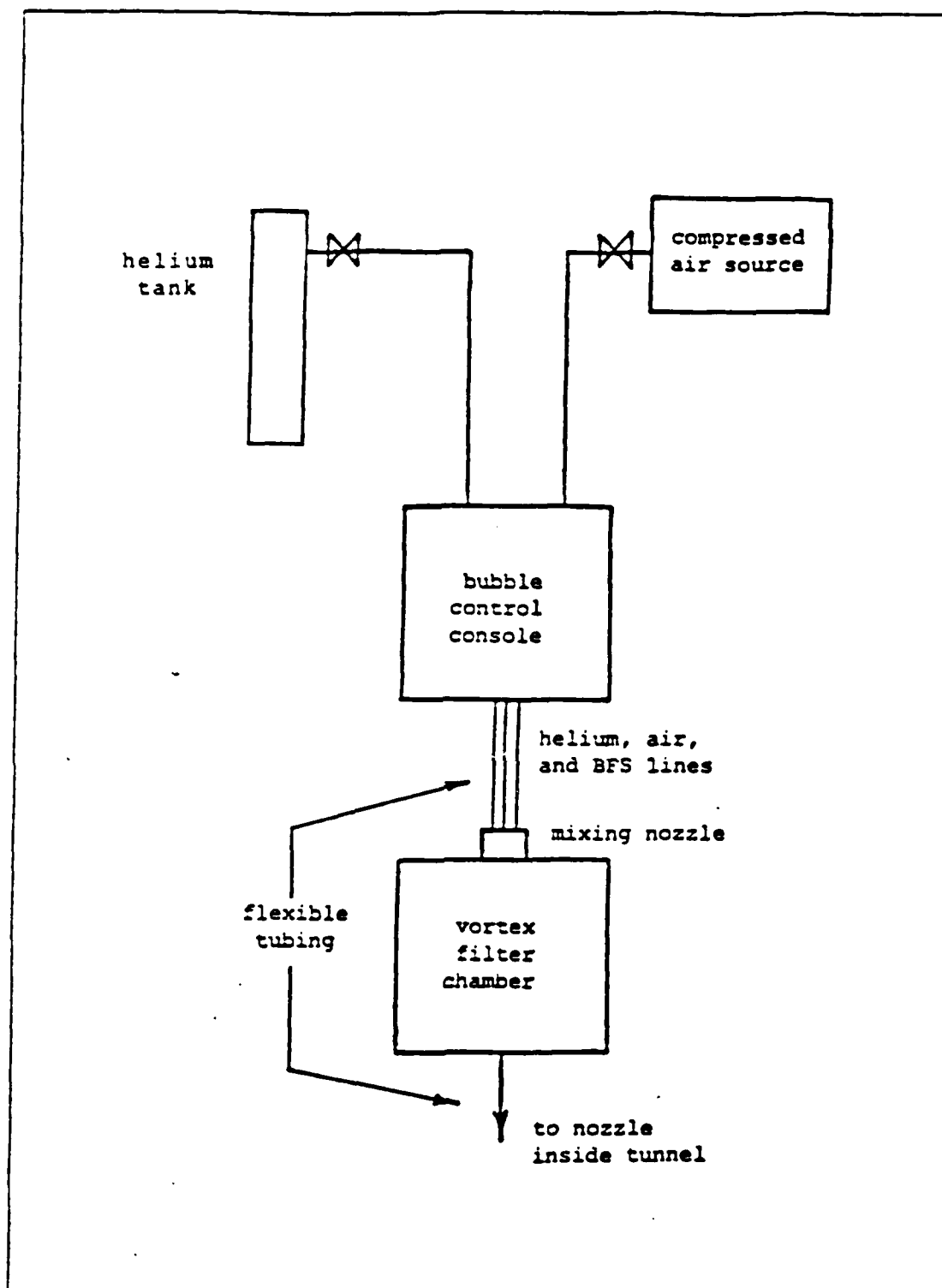


Figure 8. Diagram of the Helium Bubble System
[Biskaduros, Ref. 8]

micrometering valves at the console. The helium, bubble film solution and air exit the console via flexible tubing and are combined in a high speed head designed with three concentric rigid tubes, one for each effluent. Bubble film solution is formed into helium filled bubbles and propelled into the vortex filter chamber by 50 psi compressed air. The filter chamber is in the shape of a right circular cylinder and therefore the influx of helium bubbles forms a swirling flow. Heavy bubbles, those containing too much film solution, impact the outer wall of the chamber or fall to the chamber floor. Light bubbles impact the center tube of the chamber. Neutrally buoyant bubbles, those desired for flow visualization, exit the chamber via a rigid center tube and attached flexible tubing, and enter the environmental wind tunnel upstream of the model and immediately downstream of the previously discussed doweled turbulence generators. The bubbles physically enter the tunnel via a rigid metal "gun" made of round stock the same diameter as the doweled turbulence generators. The "gun" can be positioned to any location across the width of the tunnel floor depending on the yaw angle of the ship model.

Most problems associated with the generation of helium bubbles can be traced to clogging of the console mechanism or high speed head. To alleviate the minor nuisance the high speed head was cleaned daily, while the console and

associated tubing was flushed with warm water, filled via the 5 oz cylinder, every three to four days.

C. PHOTOGRAPHY

Proper lighting of the test section area is paramount in order to effectively photograph the helium bubble streamlines while showing an outline of the ship model for reference. Three types of lights were used during this study: 1) EIMAC model R-150-5 arc lamp, 2) Kodak Ectographic model AF-2 slide projector, and 3) Rotodisc slide projector. These lights were positioned so as to provide maximum illumination to the immediate vicinity of the LHA model flight deck while showing absolute minimum glare on the flight deck itself and adjacent superstructure.¹ Arc lamps, with a color temperature of 6000K, are preferred to projectors, with a nominal color temperature of 2500K, since the purer white light generated at 6000K provides better illumination of the helium bubbles.

The arc lamp incorporated a collimating network with an adjustable iris housed in a cylinder mounted to the arc lamp source. Collimation of the projectors was accomplished using slide mounting frames covered with aluminum tape and cut out to form narrow slits. Although this is a crude method it proved highly effective in actual use.

¹Actual light positions will be discussed in the chapters dealing with Results and Conclusions.

A professional-format Hasselblad 2000 FCW single lens reflex camera was used for this study. Although both a 110 mm and 150 mm lens were available, exclusive use of a Zeiss 150 mm f2.8 showed the finest results. Lens accessories used were a haze filter and lens hood.

Two black and white film formats were employed, Polaroid 107C 3000 ASA and Kodak TMY 120 TMAX 400. Once satisfactory lighting was achieved, a Polaroid film magazine was shot until the proper combination of f-stop and exposure time was reached. At this point film magazines were switched to one containing Kodak TMAX and print quality photographs were taken. To compensate for the difference in speed between the two film formats used, upon switching to the Kodak TMAX, shots were taken at up to three different camera settings: 1) opening an additional two f-stops and halving the exposure time, 2) opening an additional one and a half f-stops at the same exposure time, and 3) opening one additional f-stop at the same exposure time. The Kodak TMAX film was "pushed" in developing to ASA 1600. Appropriate prints were selected from proof sheets and are shown in Chapter VI.

VI. RESULTS

The results considered in this study were attained using helium bubble flow visualization, previously discussed in Chapter V. Although likewise mentioned in Chapter V, certain aspects of lighting bear emphasis in view of the photographic examples that follow in this chapter.

Early attempts by the author to photograph the LHA flow field yielded poor results. Pictures lacked contrast not only of the helium bubble streaklines, but also the hull of the ship. Any given picture displayed a dull outline of the hull form and poor light absorption by the helium bubbles. Three tactics were employed to correct this situation: 1) enlarging the swath area of helium bubbles by cross-connecting a second "gun" to the vortex filter chamber effluent, 2) replacing the existing arc lamp bulb, and 3) almost entirely restricting the use of any lighting to that which formed nearly parallel ray path lines.

Use of a second "gun" allowed the existing amount of helium bubbles to be spread out over a larger area and therefore cover more of the model. This was a necessity for yaw angles of 30 and 45 degrees where a greater beam area of the ship model was exposed to the wind.

In using arc lamps a sensitivity to their quality of light must be kept in mind. Alternate brightening and dimming of the light, as well as non crisp fringes, are

indicative of lamp wearout. These symptoms are suggestive of a gas pressurization loss in the lamp, and may be caused by rough handling or age. Upon replacement of the existing lamp, the overall intensity was noticeably increased and its output was both consistent and crisp.

Of the three tactics used, the one contributing the greatest result was that of light positioning. It was noted by trial and error that whenever light sources were arranged in a parallel, or nearly parallel fashion (i.e., all arranged astern of the model with none to the side), the picture quality was remarkably more crisp. Even with a new arc lamp bulb and a greater swath of bubbles, use of crossing light rays gave poor photographic contrast of both the ship model and helium bubbles. Initial consultation with the NPS Photo Lab revealed that this may be due to partial image cancellation through the camera lens due to crossing ray paths of the light sources. Further investigation of this optical effect may bear this out. However, this study clearly showed that the use of parallel, or nearly parallel, light sources in fact rendered noticeably superior photography when compared to those obtained using crossing ray paths.

Of all the light sources used, and previously mentioned in Chapter V, the EIMAC model R-150-5 arc lamp delivered the best quality light, both in terms of its 6000K color temperature and its crispness. Photographs appearing in

this report will clearly show the limits of the arc lamp coverage and it will be noticed that in those limits helium bubble definition is superior to that outside the limits. Helium bubble traces in the bow section of the ship model were not as noticeable in any of the yaw positions selected, when compared to the midships and stern positions. This may be attributed to the bow section's distance from the light sources, which were arranged astern of the ship model. In order not to interfere with the very flow the author was trying to qualitatively photograph, light sources had to be placed well astern of the ship model. A tradeoff in doing so was a less intense light source at the bow.

Yaw angle selection was based upon NAVAIR 00-80T-106 report [Ref. 13], delineating helicopter rotor engage/disengage and launch/recovery wind limitations for all helicopters operational on the TARAWA class LHA. Wind speed was chosen as approximately 25 knots, as was previously discussed in Chapter III, in order to define the maximum end of the wind envelopes. A review of Reference 13 showed that wind directions of 330 to 045 degrees at 25 knots would cover the overwhelming majority of the envelopes mentioned. Additionally pitch and roll limitations of 1.1° pitch and 6° roll, discussed in Chapter III, were used. With these parameters in mind, the following combinations were photographed for yaw angles of 0° , 45° port and 30° starboard:

- 1) 0° pitch/ 0° roll
- 2) 1.1° pitch up/ 0° roll
- 3) 0° pitch/ 6° port roll
- 4) 1.1° pitch up/ 6° port roll
- 5) 0° pitch/ 6° starboard roll
- 6) 1.1° pitch up/ 6° starboard roll.

Due to the size of the model used, and the need for photographs of sufficient clarity with respect to size, the model was divided up into three sections, bow, midships and stern. Each of the combinations listed above were shot for each section at each yaw angle for a total of 54 different poses photographed. All photographs were taken using a 150 mm lens. Figure 9 shows a presentation of the LHA flight deck indicating the helicopter landing spots numbered 1 through 9. Correlation of ship section with spots is as follows:

- 1) bow: spot 1, 2, 3, 3a, 4
- 2) midships: spot 5, 6, 7
- 3) stern: spot 8, 9

Throughout the course of the study, wind tunnel speed was verified using an EDM 2500C micromanometer with a sensing point at 30 inches off the tunnel floor. In this manner the ABL, discussed in Chapter II and experimentally derived as noted in Chapter IV, could be checked for consistency.

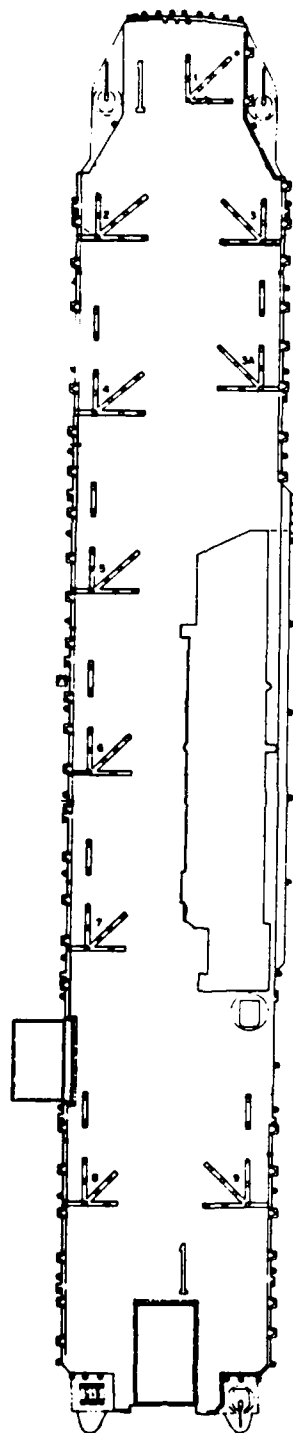


Figure 9. LHA Flight Deck with Helicopter Spots [Ref. 14]

A. ZERO DEGREE YAW

As reasonable expectations would dictate, the zero degree yaw angle displayed a relatively smooth and quite symmetrical flow pattern. 0° pitch and roll are displayed in Figures 10, 11 and 12. The bow section, Figure 10, indicates that the flow over the bow has no evidence of flow detachment. However, the bow shows evidence of a trailing vortex structure in the streaklines. Midships and stern sections, Figures 11 and 12, have little such evidence and exhibit an extremely smooth flow pattern.

Figures 13, 14 and 15 capture bow, midships and stern displays of 1.1° pitch up and 0° roll. Although quite similar to the 0° pitch and roll presentations, the bow section, Figure 13, shows a more defined trailing vortex structure. This vortex is damped by the time the midships section, Figure 14, is reached. However a comparison to the midships section for 0° pitch and roll, Figure 11, indicates a perceptible difference in the streaklines, showing a slight residual of the bow trailing vortex. The stern section, Figure 15, compares virtually identically to the case for 0° pitch and roll.

0° pitch, 6° port roll, Figures 16, 17 and 18, can easily be confused with the attitudes discussed above. Indeed there is little difference in the streaklines displayed.



Figure 10. 0° Yaw: 0° Pitch, 0° Roll, Bow

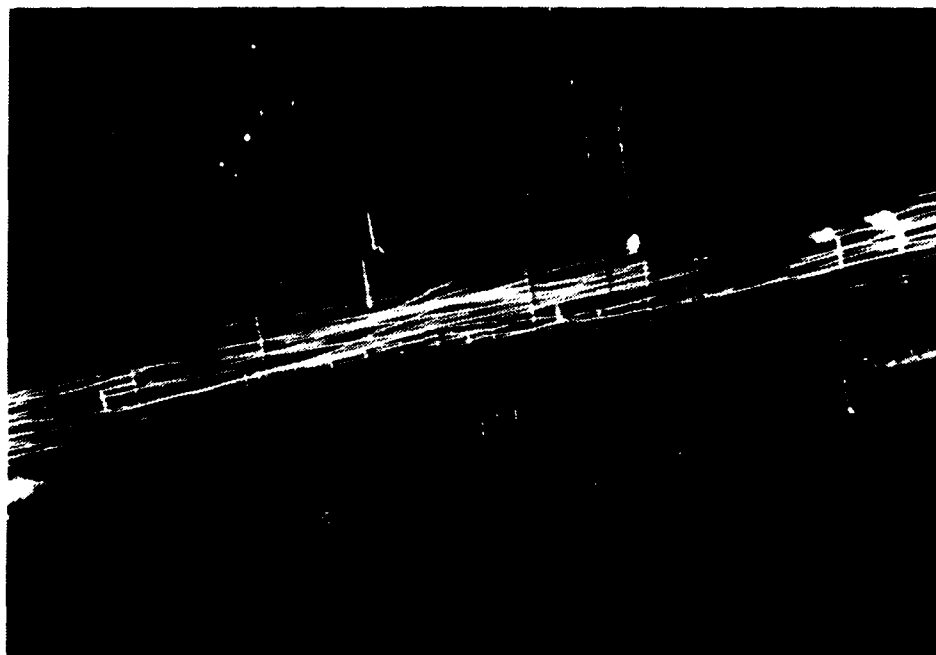


Figure 11. 0° Yaw: 0° Pitch, 0° Roll, Midships



Figure 12. 0° Yaw: 0° Pitch, 0° Roll, Stern

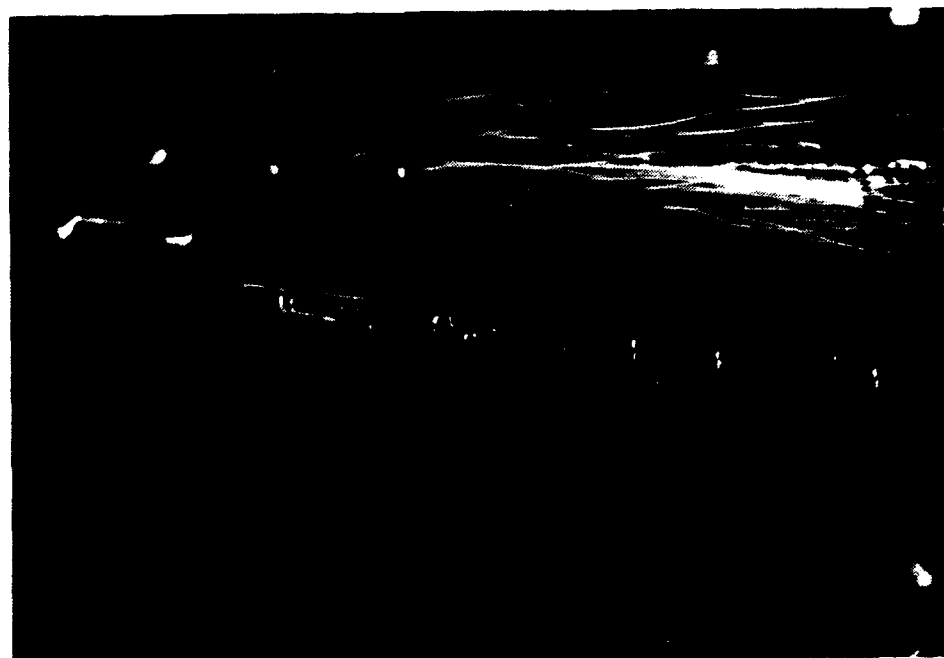


Figure 13. 0° Yaw: 1.1° Pitch Up, 0° Roll, Bow

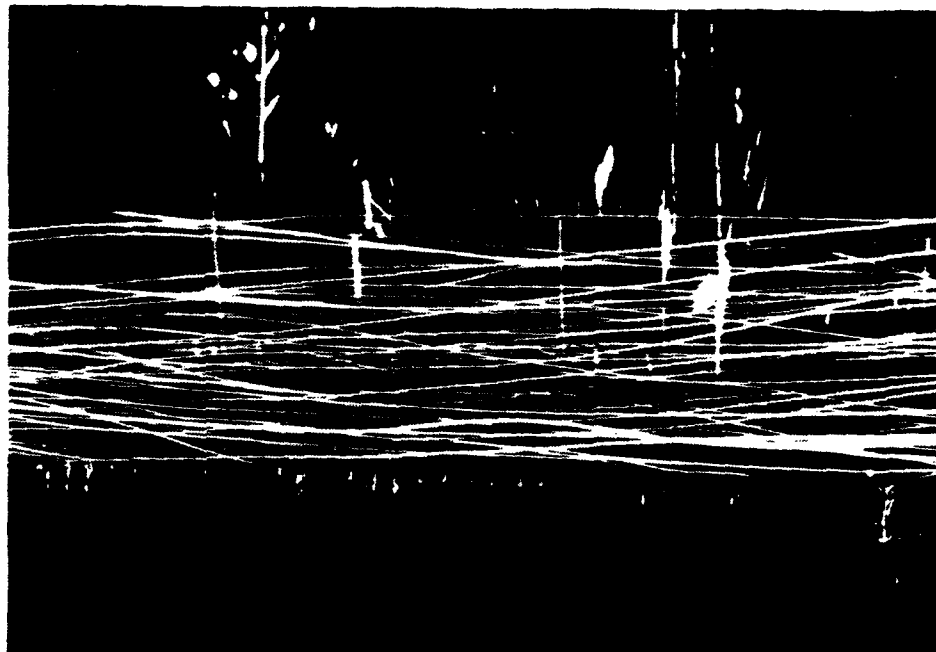


Figure 14. 0° Yaw: 1.1° Pitch Up, 0° Roll, Midships

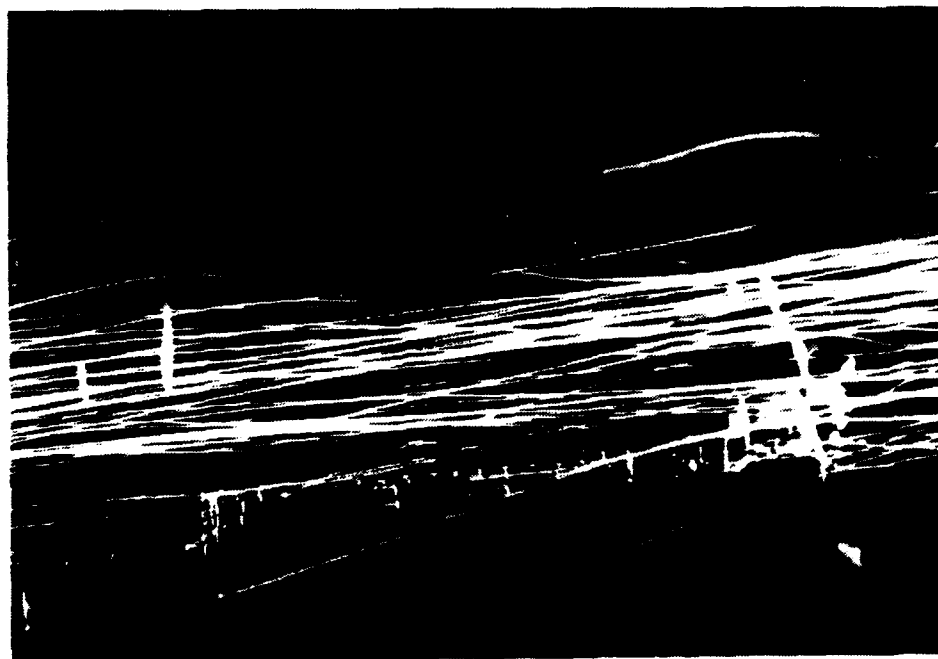


Figure 15. 0° Yaw: 1.1° Pitch Up, 0° Roll, Stern

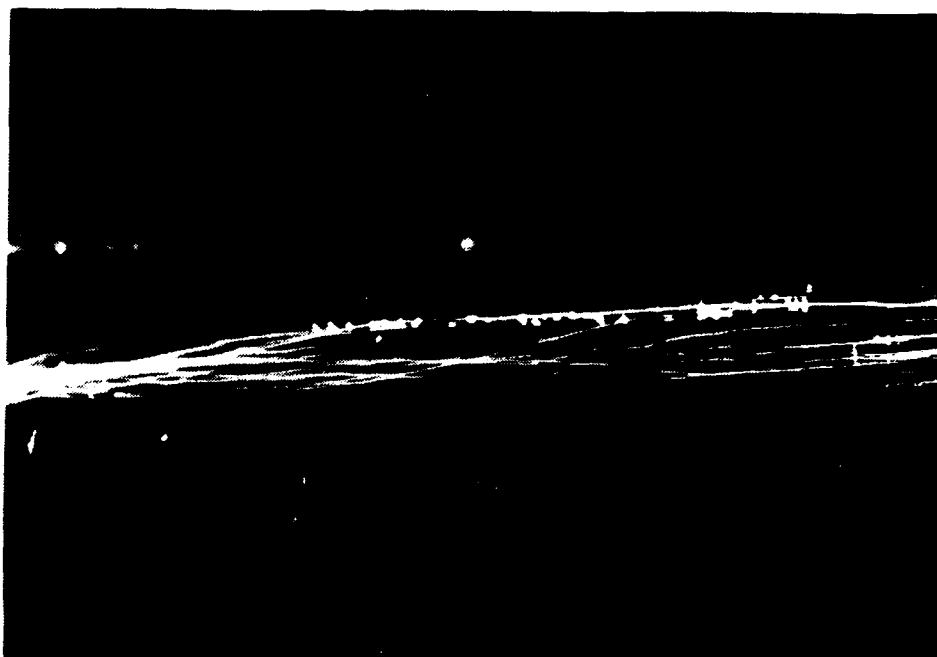


Figure 16. 0° Yaw: 0° Pitch, 6° Port Roll, Bow



Figure 17. 0° Yaw: 0° Pitch, 6° Port Roll, Midships



Figure 18. 0° Yaw: 0° Pitch, 6° Port Roll, Stern

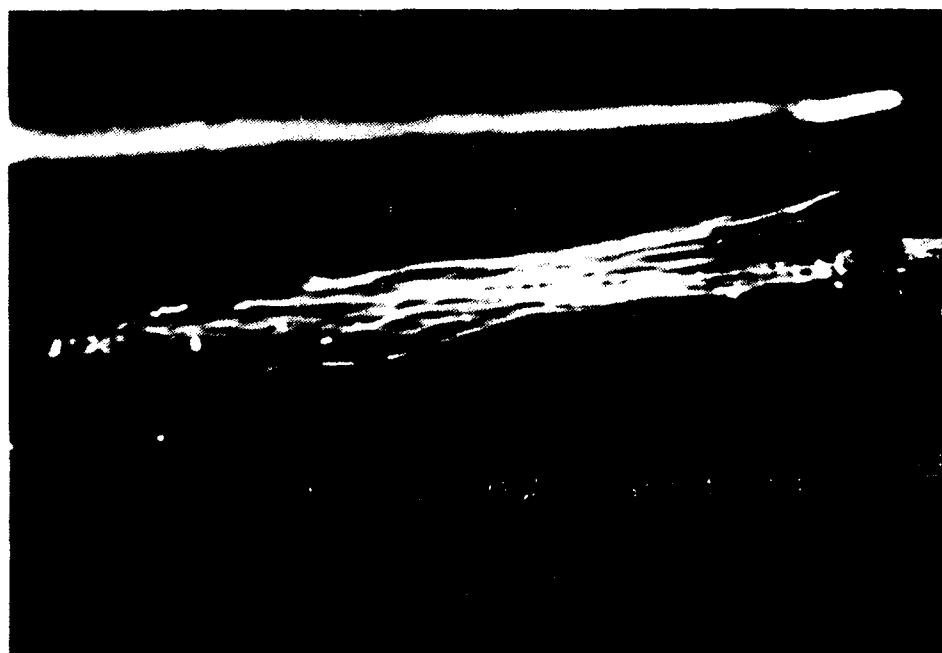


Figure 19. 0° Yaw: 1.1° Pitch Up, 6° Port Roll, Bow

1.1° pitch up, 6° port roll, Figures 19, 20 and 21, likewise exhibit similar streakline patterns. However, when comparing the bow section photograph of 1.1° pitch up, 6° port roll, Figure 19, to that of 0° pitch, 6° port roll, Figure 16, a perceptible difference in the trailing vortex pattern once again is in evidence. As was noted in the previous case, the 1.1° pitch up presentation does show a more defined vortex structure pattern.

Figures 22, 23 and 24 document the 0° pitch, 6° starboard roll attitude. Similar comments, as discussed for previous 0° pitch presentations, are germane to this attitude.

Concluding the 0° yaw angle description, Figures 25, 26 and 27 display 1.1° pitch up, 6° starboard roll. The bow section, Figure 25, once again shows a more defined trailing vortex structure. Thus a pattern is established in that for each of the cases photographed, the 1.1° pitch up attitude exhibits a similarly more established trailing vortex when compared to the 0° pitch attitude. Several photographs, most notably Figures 10, 13, 16, 19, 22 and 25 show a streakline pattern above that of the vortex structure. This is evaluated as flow that does not contact the hull form. However, it is influenced by the presence of the hull.

B. FORTY-FIVE DEGREE PORT YAW

While the 0° yaw presentations were less than exciting in their results, this is more than adequately compensated

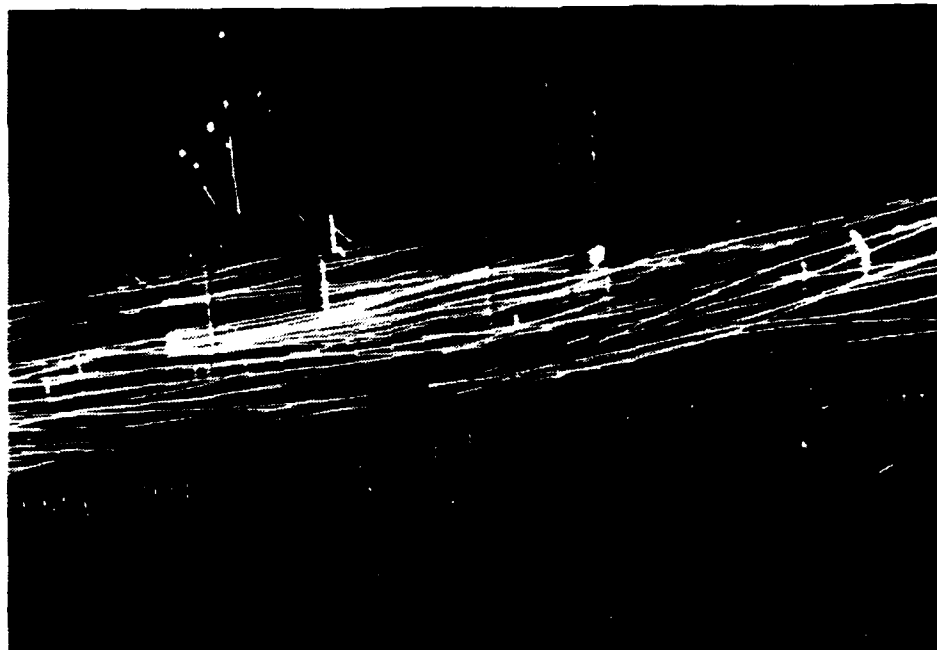


Figure 20. 0° Yaw: 1.1° Pitch Up, 6° Port Roll, Midships

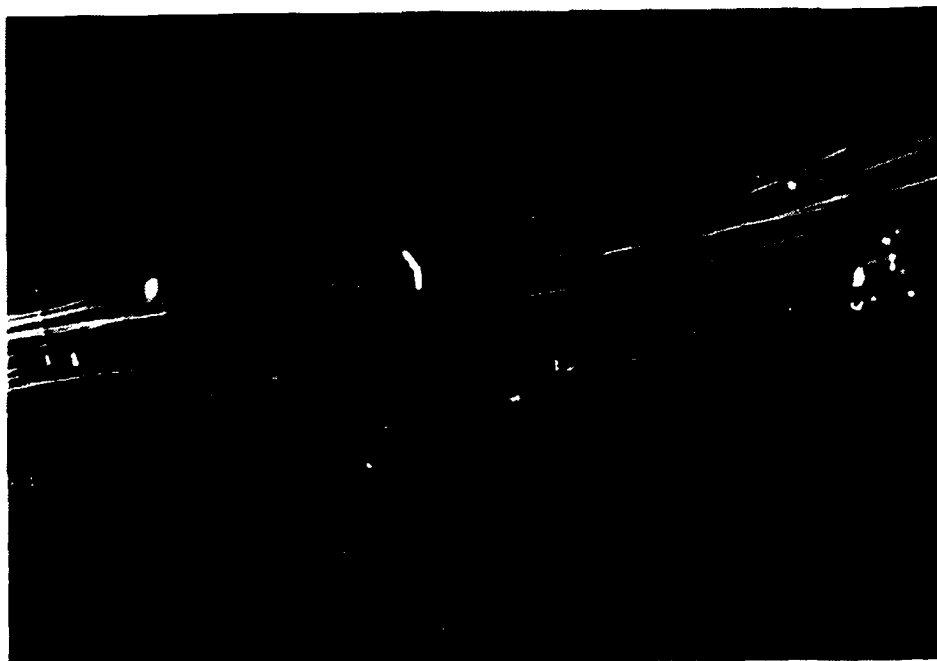


Figure 21. 0° Yaw: 1.1° Pitch Up, 6° Port Roll, Stern

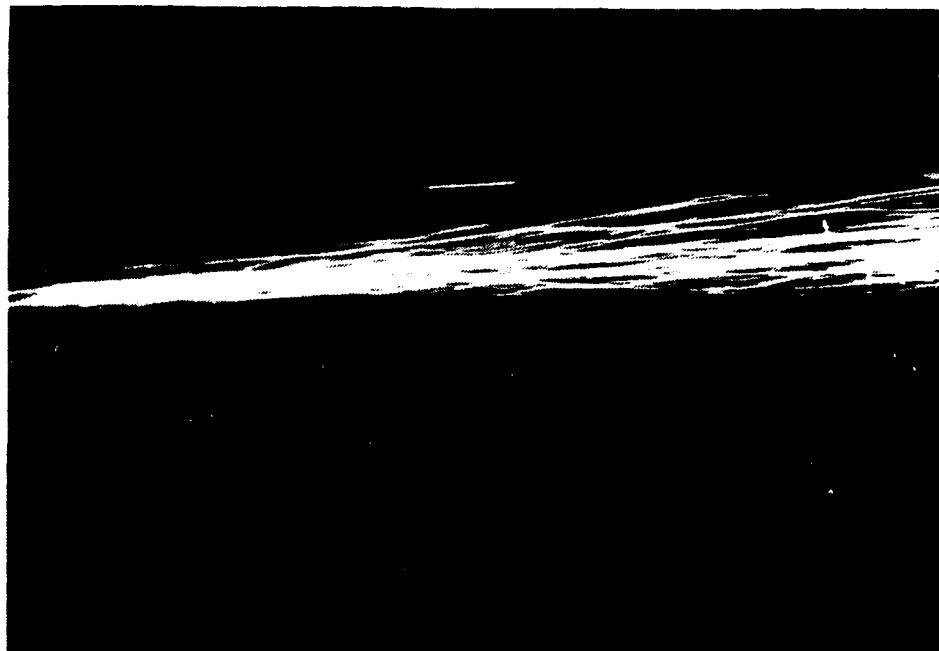


Figure 22. 0° Yaw: 0° Pitch, 6° Stbd Roll, Bow

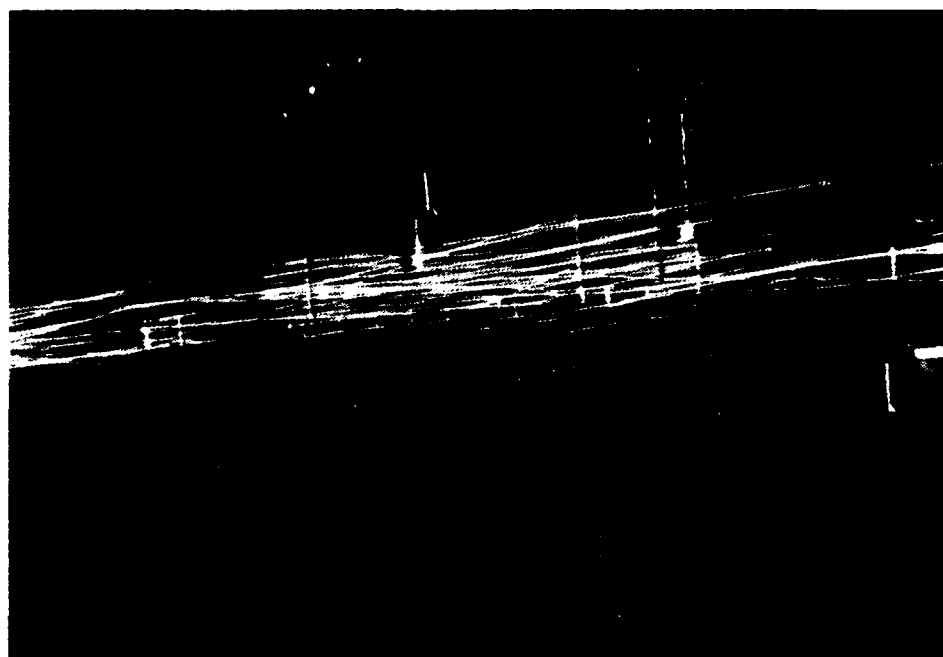


Figure 23. 0° Yaw: 0° Pitch, 6° Stbd Roll, Midships

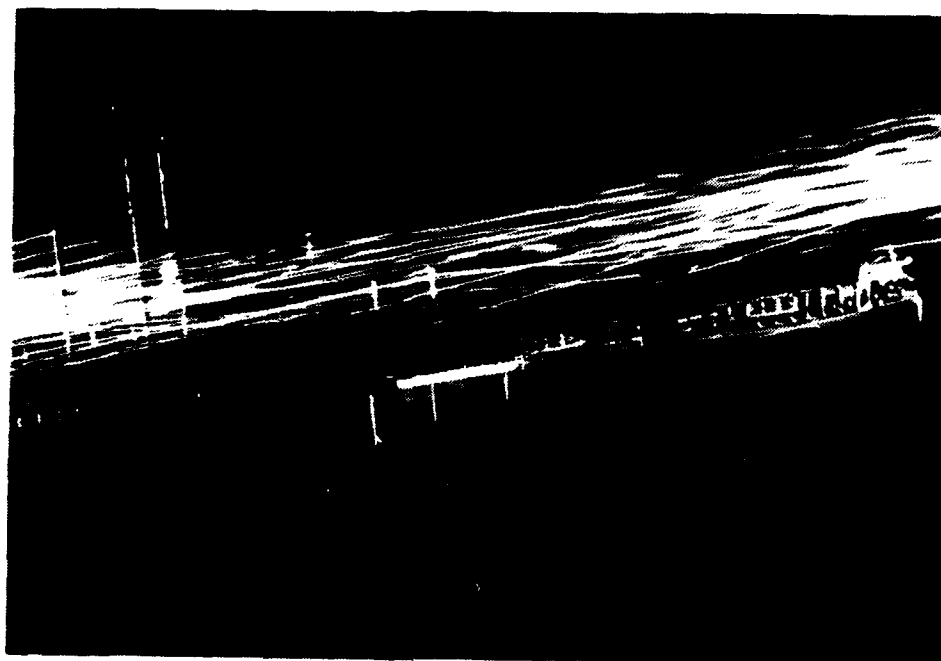


Figure 24. 0° Yaw: 0° Pitch, 6° Stbd Roll, Stern

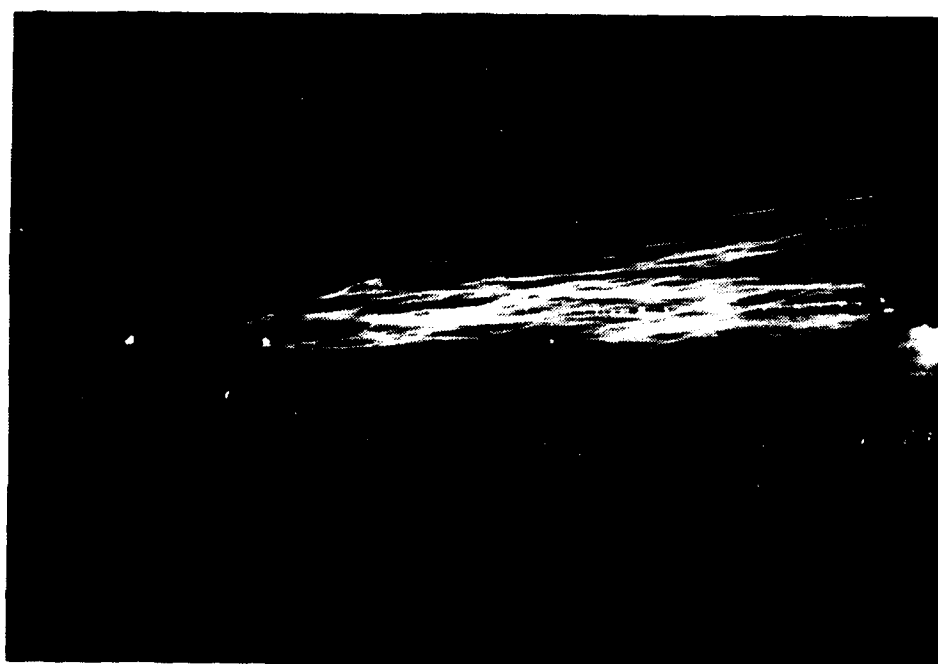


Figure 25. 0° Yaw: 1.1° Pitch Up, 6° Stbd Roll, Bow

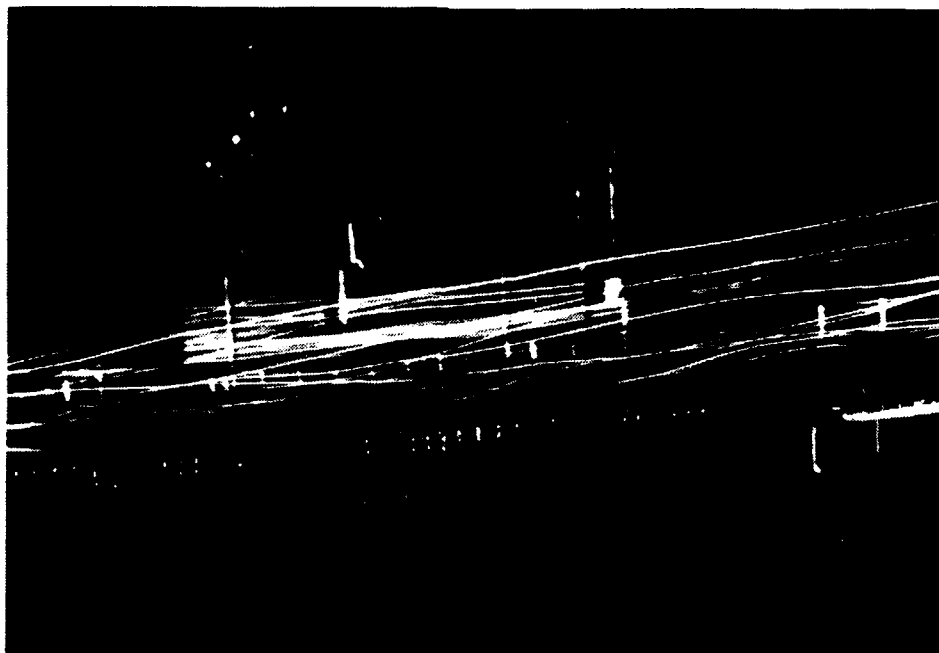


Figure 26. 0° Yaw: 1.1° Pitch Up, 6° Stbd Roll, Midships

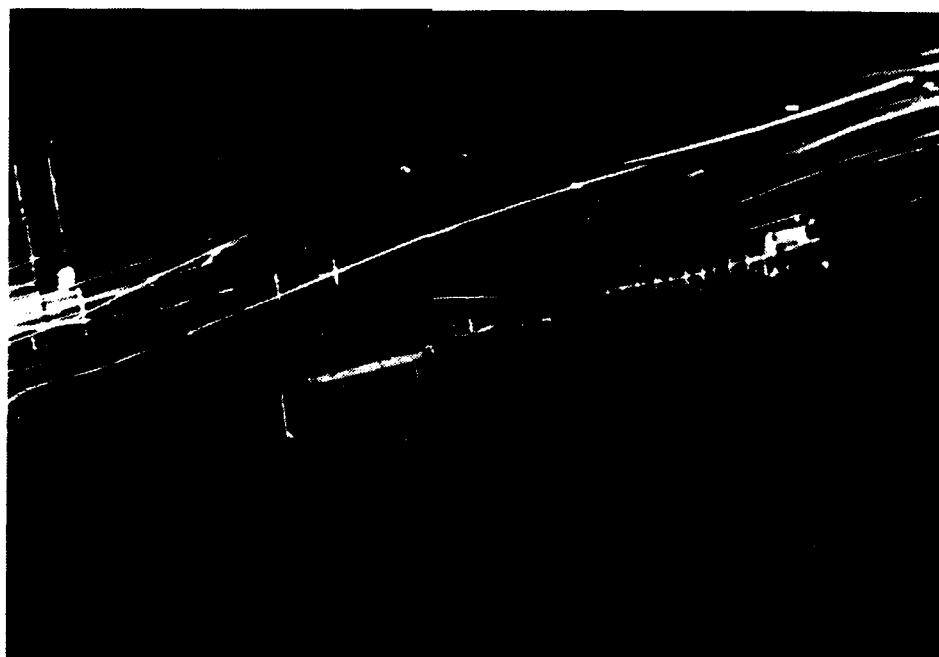


Figure 27. 0° Yaw: 1.1° Pitch Up, 6° Stbd Roll, Stern

for by the 45° port yaw photographs. The cross flow interference created by the superstructure, located on the windward side of the ship, lends itself to some spectacular photographs most notably in the midships section of all the attitudes displayed. Of particular interest are the areas of reversed flow and turbulence so clearly evident in the midships and stern sections. In general the flow is more disturbed and complex and the trailing vortex structure is no longer symmetrical. Again, the bow section however shows no evidence of flow detachment but does show a larger trailing vortex structure in the streaklines.

Figures 28, 29 and 30 represent 0° pitch and roll. The bow section, Figure 28, shows the most symmetrical pattern of all the sections displayed. As mentioned before, evidence of a trailing vortex exists. The midships and stern sections show extremely complex flows caused by turbulent vortex formation as the flow rolls over and around the superstructure. The vortices tend to be pulled down and combine on the leeward (downward) side of the ship after they exit the deck edge of the flight deck. These two sections have noticeable reversed flow regions and recirculating zones.

1.1° pitch up, 0° roll, Figures 31, 32 and 33 are similar in appearance to the photographs of 0° pitch and roll. However, as was the case for the 0° yaw presentations, the 1.1° pitch up attitude exhibits a larger trailing vortex

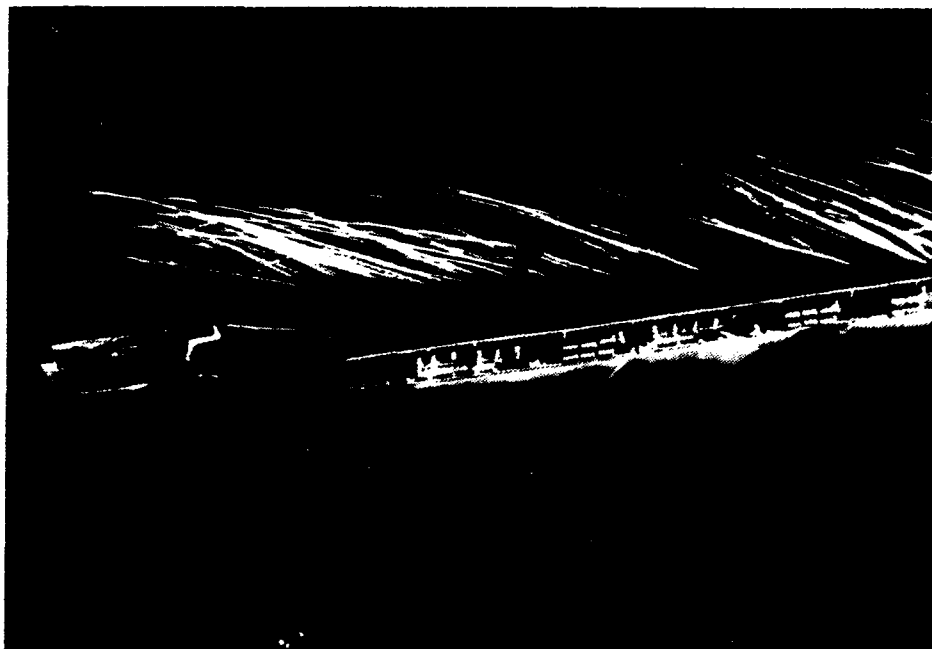


Figure 28. 45° Port Yaw: 0° Pitch, 0° Roll, Bow

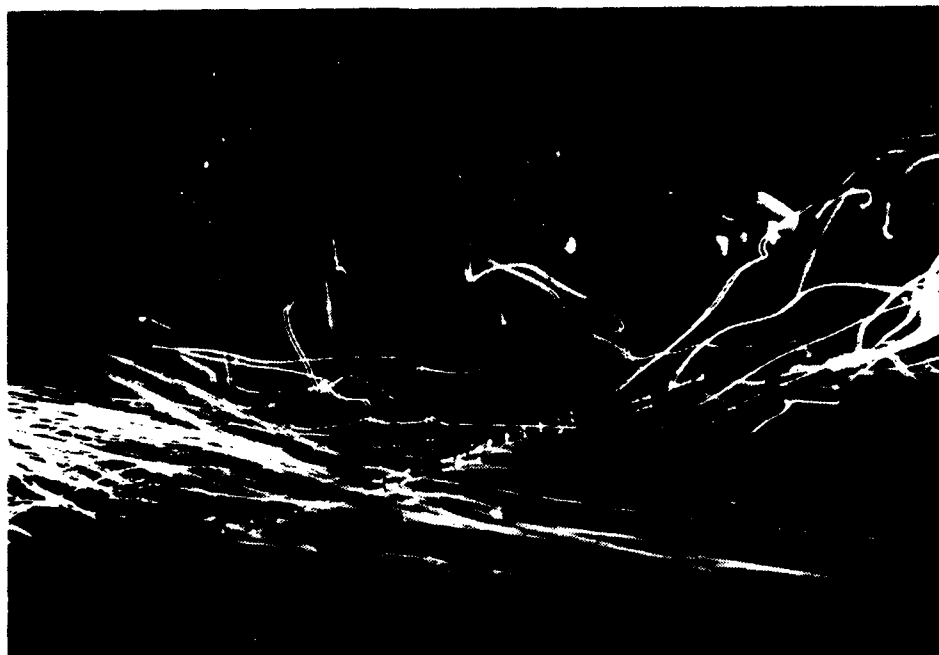


Figure 29. 45° Port Yaw: 0° Pitch, 0° Roll, Midships

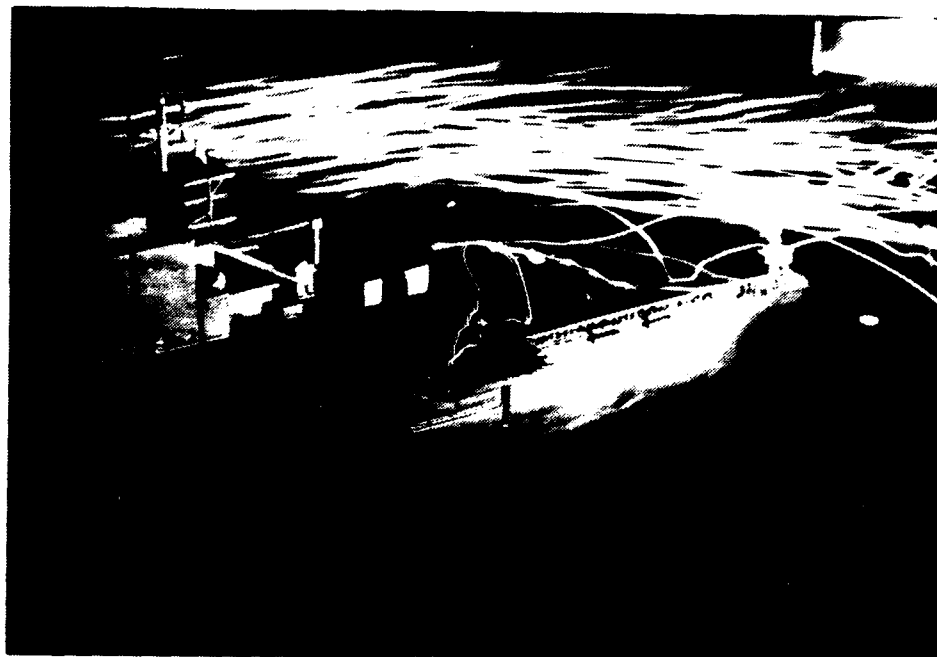


Figure 30. 45° Port Yaw: 0° Pitch, 0° Roll, Stern

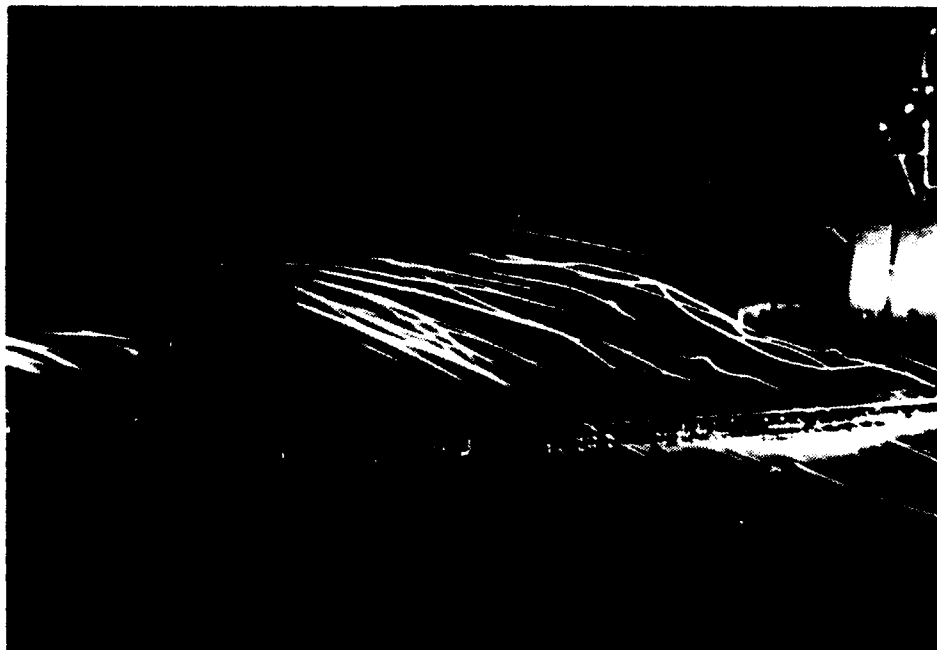


Figure 31. 45° Port Yaw: 1.1° Pitch Up, 0° Roll, Bow

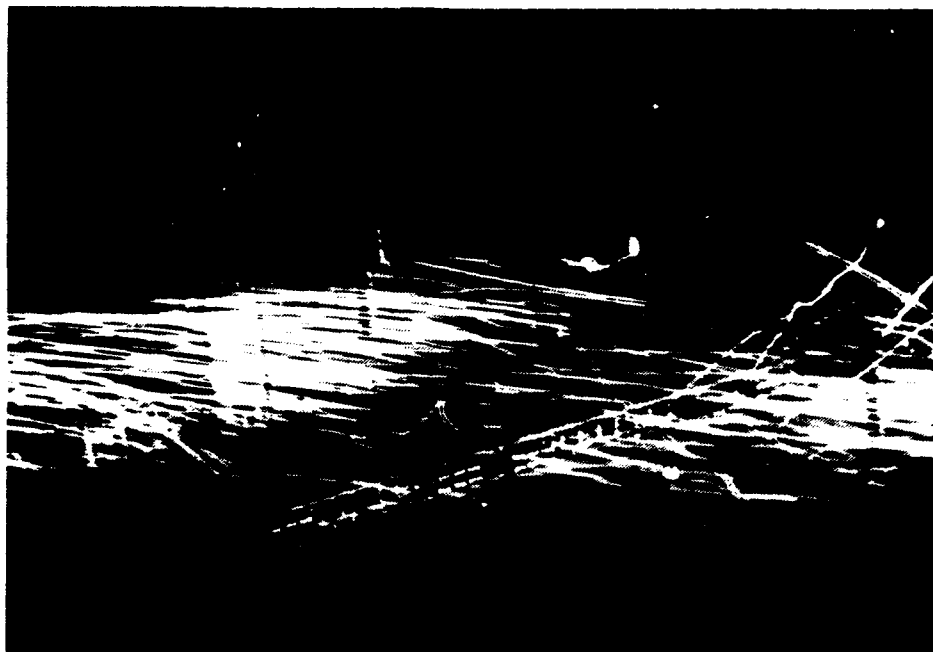


Figure 32. 45° Port Yaw: 1.1° Pitch Up, 0° Roll, Midships

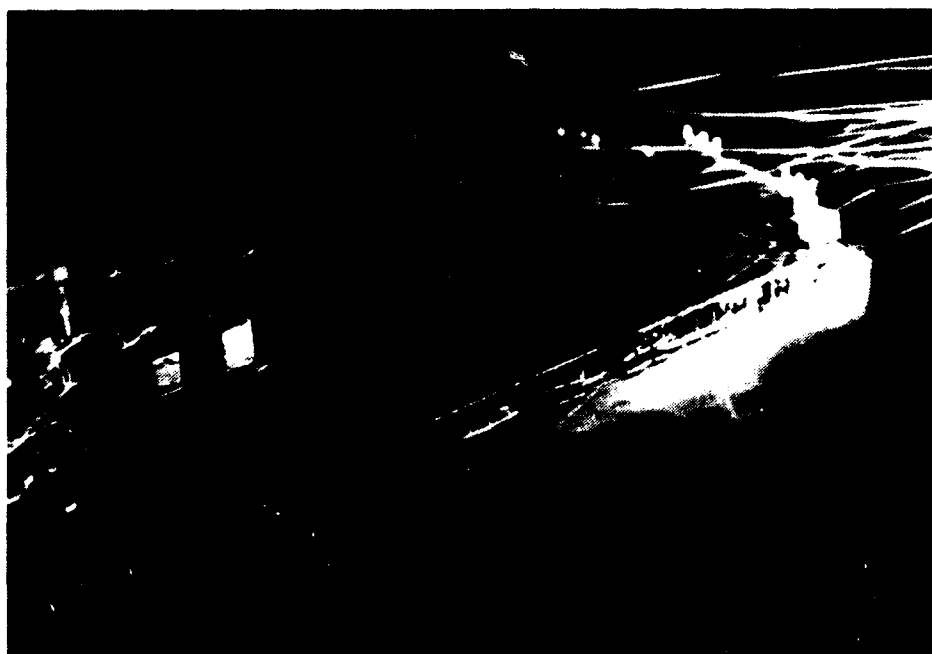


Figure 33. 45° Port Yaw: 1.1° Pitch Up, 0° Roll, Stern

structure on the bow, Figure 31. Midships and stern records, Figures 32 and 33, again show extremely complex and turbulent flow with areas of reversed flow.

A plausible prediction of port roll attitudes in a 45° port yaw would be that vortices would be more in evidence. One would reasonably expect this because the port roll is away from the wind direction and therefore even more of the hull form is subjected to the wind's influence. Figures 34, 35 and 36 depict 0° pitch, 6° port roll. As expected, even the bow section, Figure 34, previously showing no flow detachment, exhibits a small scale flow detachment and turbulence. The midships and stern sections, Figures 35 and 36, are nearly indistinguishable from those previously discussed for the 45° port yaw.

1.1° pitch up, 6° port roll, Figures 37, 38 and 39, once again mirror those of 0° pitch, 6° port roll. As was previously the case, the results on the bow are slightly more intense; in this case a more intense flow detachment with turbulence, yet clearly not as intense as those of the midships and stern sections. An extensive reversed flow and recirculation region is in evidence on the stern, Figure 39.

As a corollary to the 6° port roll, the 6° starboard roll causes less of the hull form to be exposed. Therefore one would reasonably predict that this would decrease the extent of the detached flow on the bow. Evidence that this is indeed the case can be seen in Figures 40, 41 and 42 for

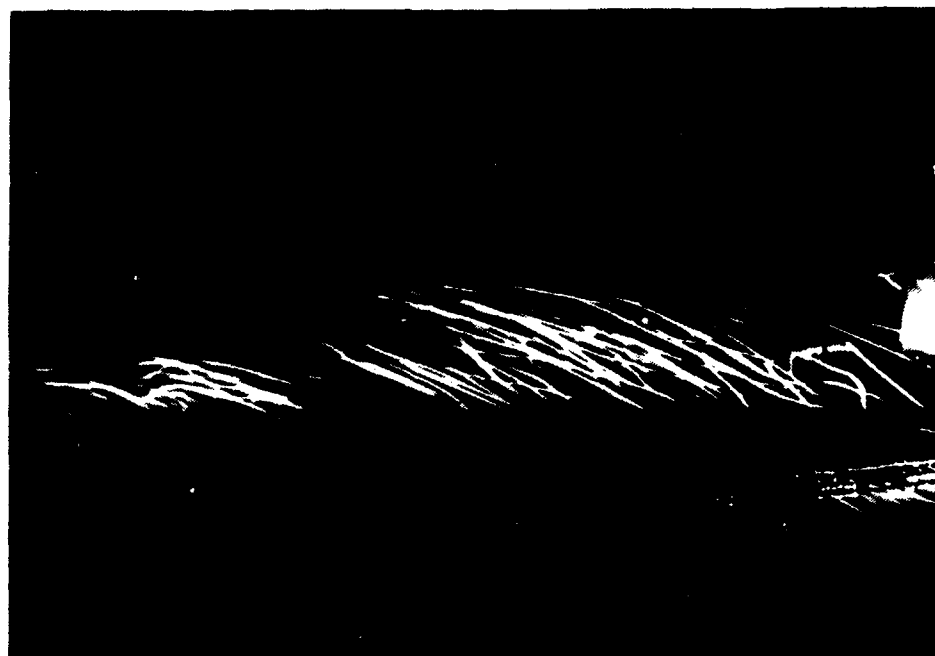


Figure 34. 45° Port Yaw: 0° Pitch, 6° Port Roll, Bow



Figure 35. 45° Port Yaw: 0° Pitch, 6° Port Roll, Midships

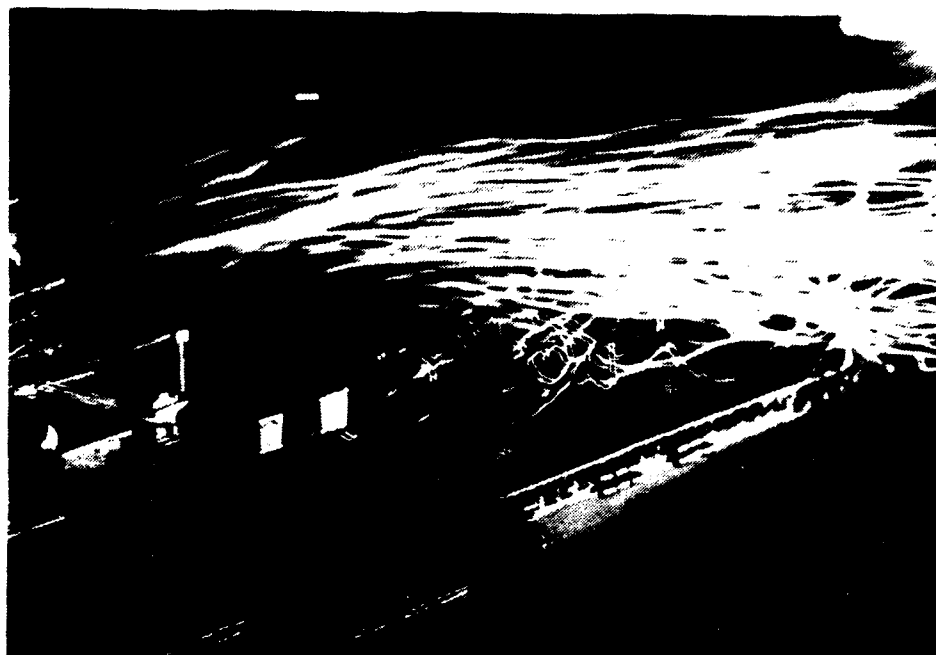


Figure 36. 45° Port Yaw: 0° Pitch, 6° Port Roll, Stern



Figure 37. 45° Port Yaw: 1.1° Pitch Up, 6° Port Roll, Bow

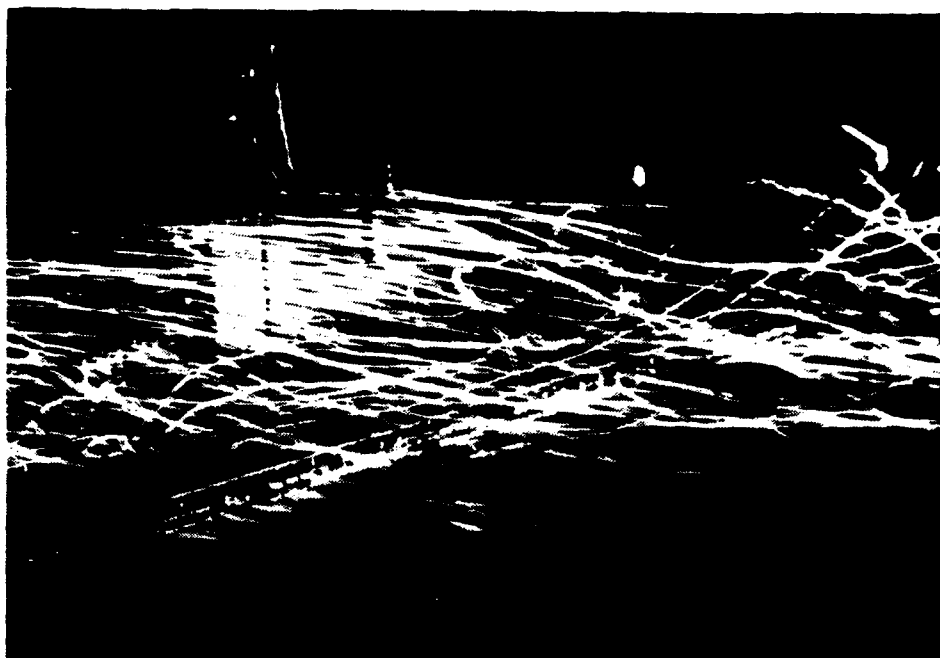


Figure 38. 45° Port Yaw: 1.1° Pitch Up, 6° Port Roll, Midships



Figure 39. 45° Port Yaw: 1.1° Pitch Up, 6° Port Roll, Stern



Figure 40. 45° Port Yaw: 0° Pitch, 6° Stbd Roll, Bow

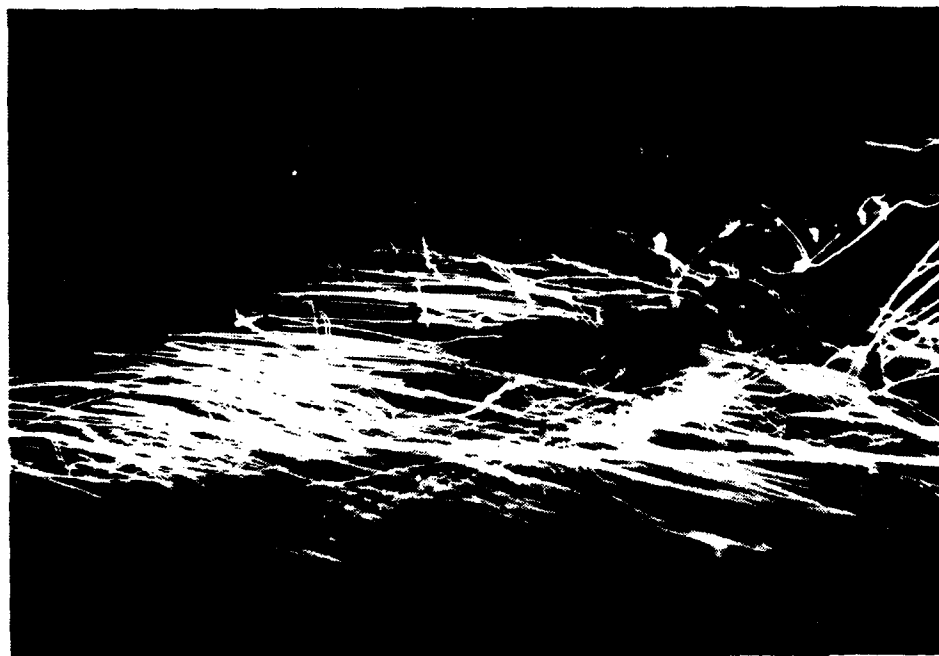


Figure 41. 45° Port Yaw: 0° Pitch,
 6° Stbd Roll, Midships

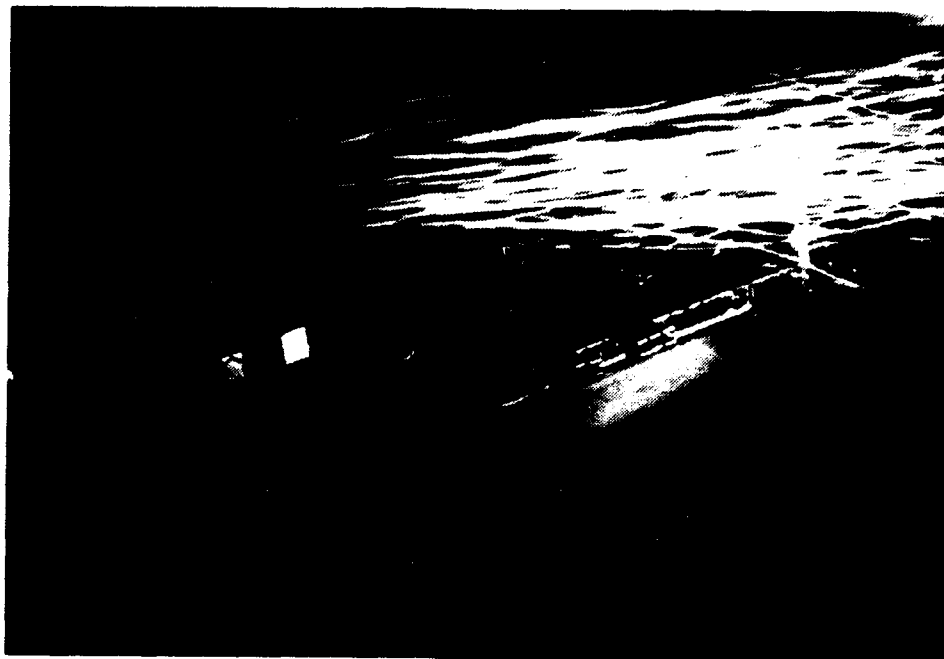


Figure 42. 45° Port Yaw: 0° Pitch, 6° Stbd Roll, Stern

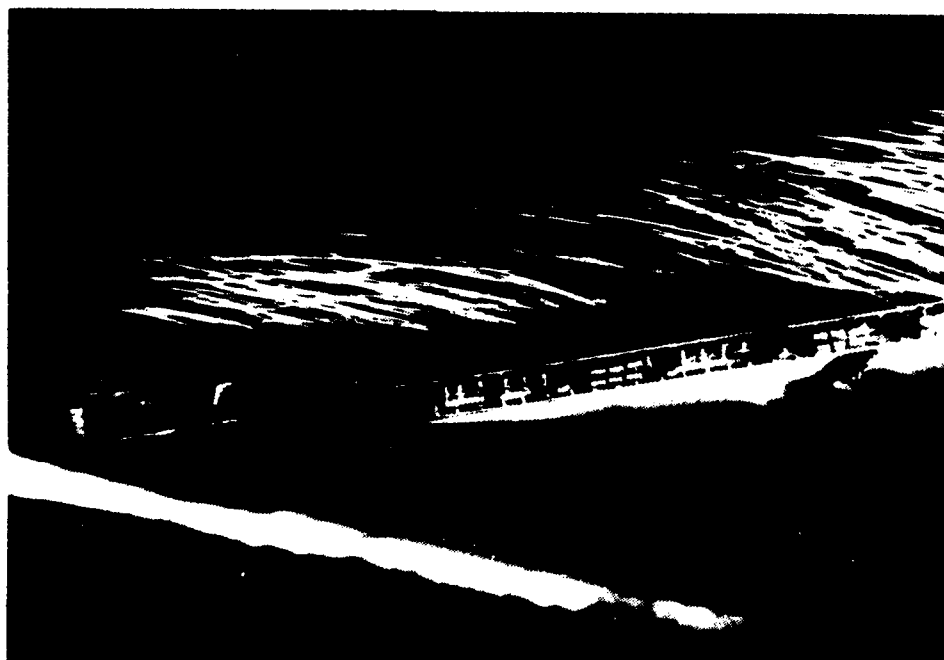


Figure 43. 45° Port Yaw: 1.1° Pitch Up, 6° Stbd Roll, Bow

0° pitch, 6° starboard roll. The bow section, Figure 40, when compared to 0° pitch, 6° port roll, Figure 34, shows almost no flow detachment yet does exhibit the trailing vortex structure. Once again, midships and stern sections, Figures 41 and 42, are areas of both reversed flow, turbulence and recirculation caused by the predominance of the superstructure.

Figures 43, 44 and 45 depict 1.1° pitch up, 6° starboard roll. Of particular note is the trailing vortex still in evidence in the midships section. The pattern of stronger trailing vortex with the 1.1° pitch up attitudes, first observed for the 0° yaw positions, has been consistent for the 45° port yaw positions.

C. THIRTY DEGREE STARBOARD YAW

The final presentation of 30° starboard yaw produced good photographic results although not as dramatic as those observed for 45° port yaw. In this case the superstructure is located on the leeward side of the ship. Therefore any resulting turbulent vortex structure that rolled off of the superstructure was not in contact with the flight deck area, but rather was located in areas clear of the starboard side of the ship and of little concern to this study due to the approach vectors used by helicopters. In general the flow over the deck was relatively smooth. Attempts were made, at several different combinations of pitch and roll, to observe any flow detachment as the helium bubbles rolled up and over

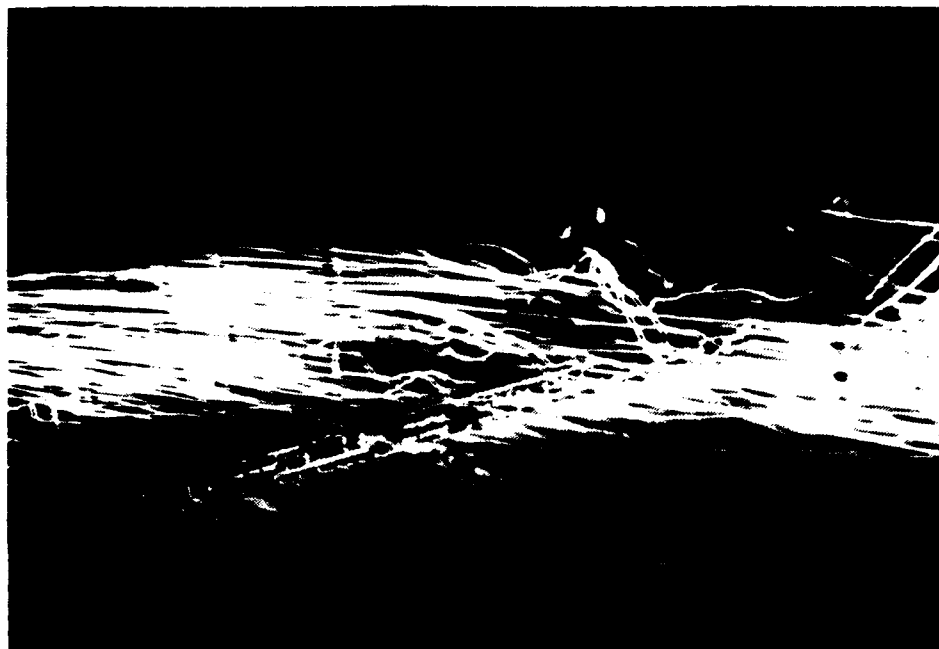


Figure 44. 45° Port Yaw: 1.1° Pitch Up,
 6° Stbd Roll, Midships

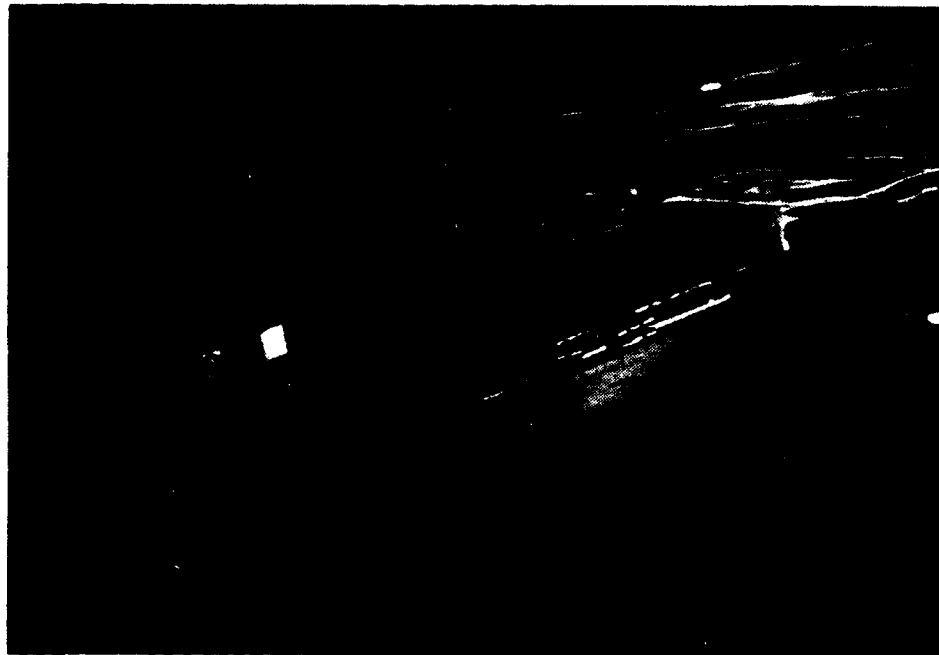


Figure 45. 45° Port Yaw: 1.1° Pitch Up, 6° Stbd Roll, Stern

the port side deck edge of the flight deck. This was accomplished by directing the flow of bubbles from the "gun" to a target point on the model much closer to the waterline. Photographic results show no flow separation. A common point shared with other yaw attitudes is the formation of a trailing vortex structure. Again, these are not pronounced but none the less visible without too much photographic interpretation.

Figures 46, 47 and 48 depict 0° pitch and roll attitudes. Bow, midships and stern poses all show smooth flow patterns with no areas of detached flow. Although these may seem less exciting to one primarily interested in fluid flow, from the perspective of a helicopter pilot these views show ideal landing conditions.

1.1° pitch up, 0° roll, Figures 49, 50 and 51 are almost identical to those depicted for 0° pitch and roll. Consistently, as before, trailing vortices are in evidence on the bow, Figure 49, while the midships and stern sections, Figures 50 and 51, display a smooth streamline structure.

Little difference in flow patterns is observed when studying 0° pitch, 6° port roll, shown in Figures 52, 53 and 54. Again, this should be expected since this represents a roll into the wind resulting in less hull form exposed to the wind. Flow is again smooth, with no detachment visible. The stern section, Figure 54, is particularly smooth,

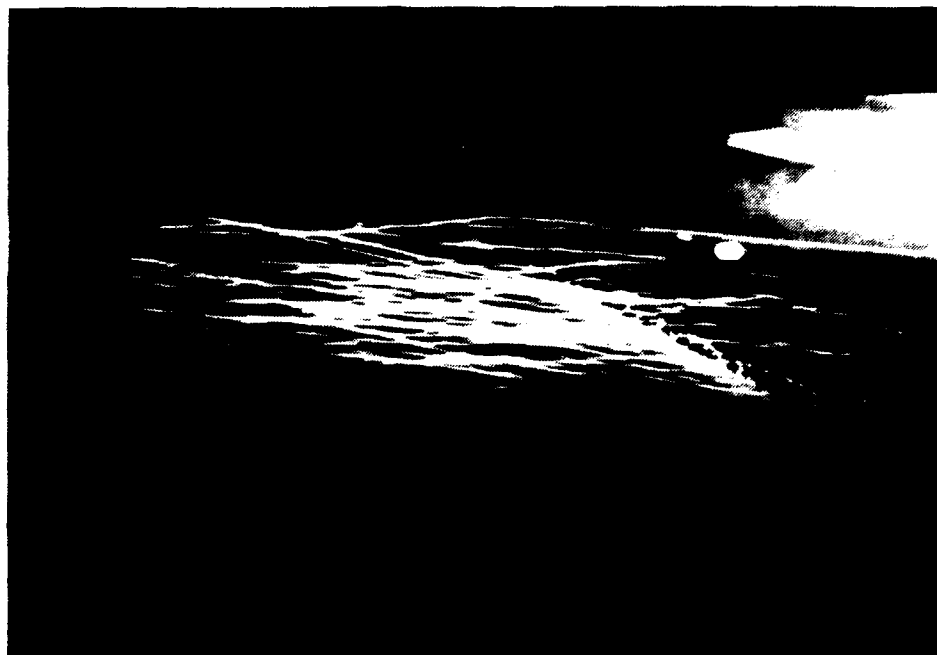


Figure 46. 30° Stbd Yaw: 0° Pitch, 0° Roll, Bow



Figure 47. 30° Stbd Yaw: 0° Pitch, 0° Roll, Midships

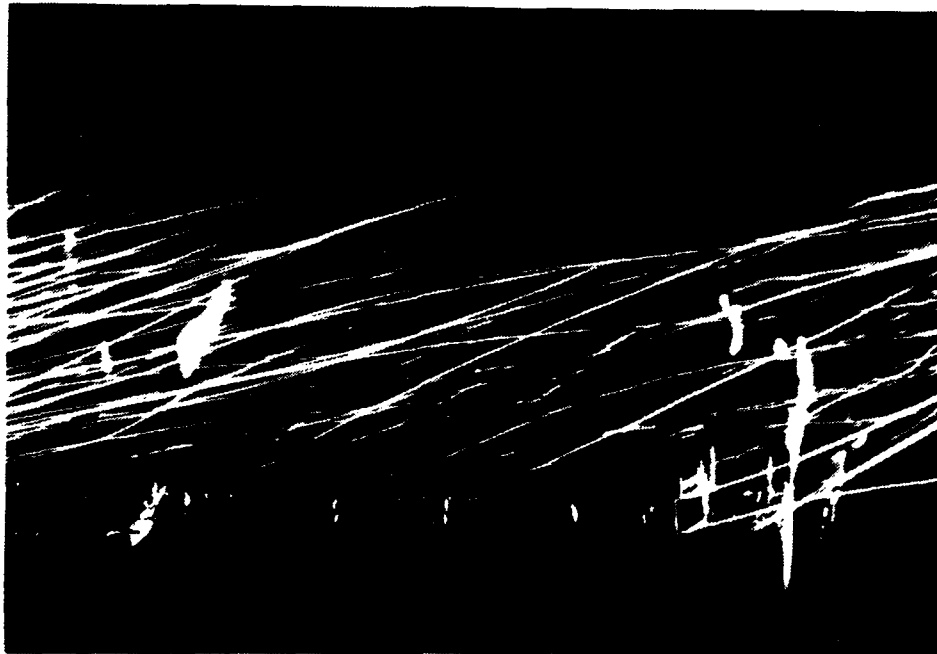


Figure 48. 30° Stbd Yaw: 0° Pitch, 0° Roll, Stern

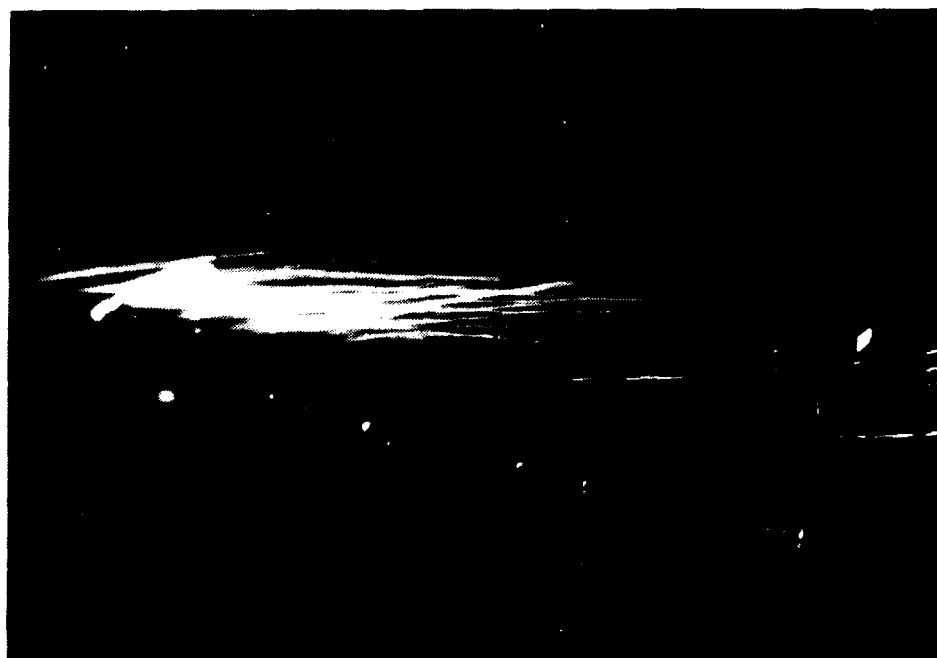


Figure 49. 30° Stbd Yaw: 1.1° Pitch Up, 0° Roll, Bow



Figure 50. 30° Stbd Yaw: 1.1° Pitch Up, 0° Roll, Midships



Figure 51. 30° Stbd Yaw: 1.1° Pitch Up, 0° Roll, Stern

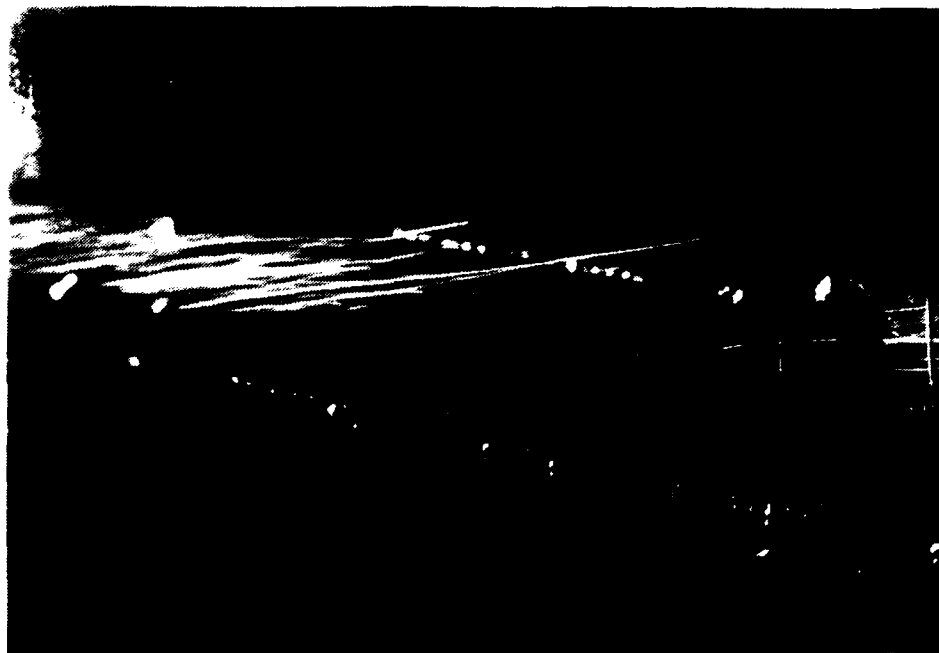


Figure 52. 30° Stbd Yaw: 0° Pitch, 6° Port Roll, Bow

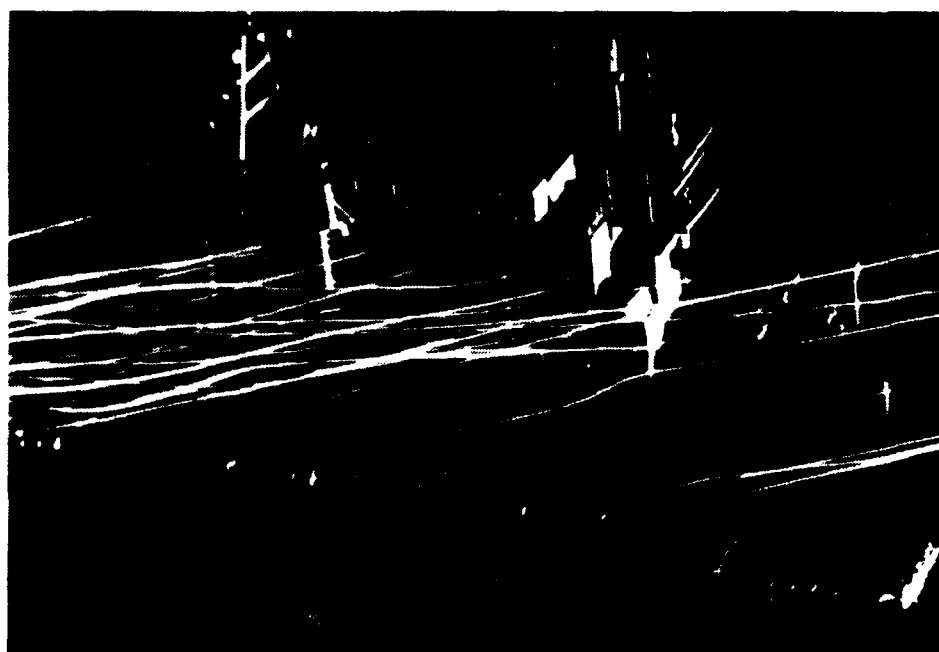


Figure 53. 30° Stbd Yaw: 0° Pitch, 6° Port Roll, Midships



Figure 54. 30° Stbd Yaw: 0° Pitch, 6° Port Roll, Stern

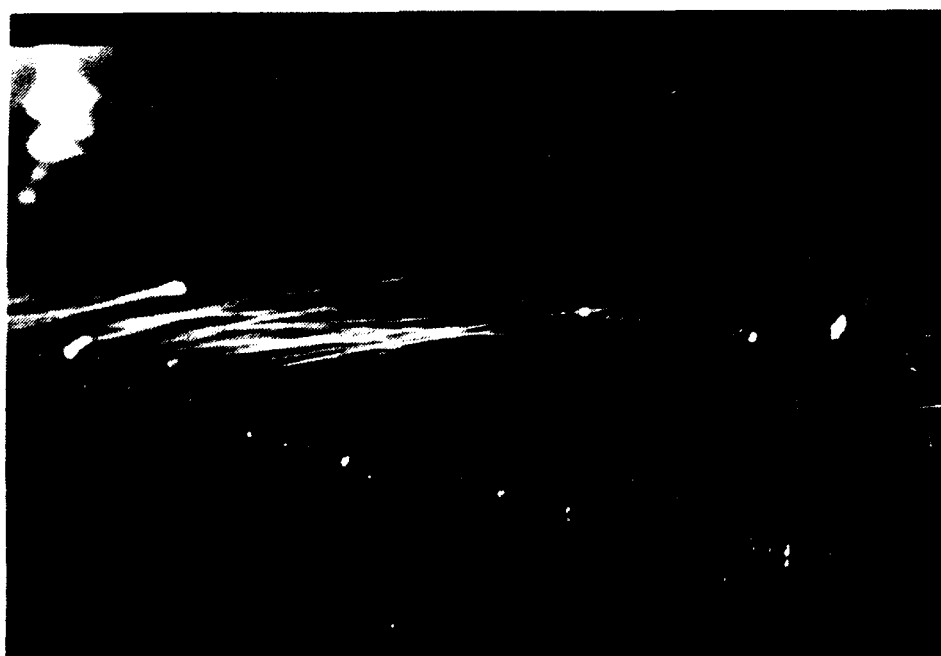


Figure 55. 30° Stbd Yaw: 1.1° Pitch Up, 6° Port Roll, Bow

showing no evidence of detached flow from the after position of the superstructure.

Figures 55, 56 and 57 represent 1.1° pitch up, 6° port roll. Once again, bow and midships sections, Figures 56 and 57, display trailing vortices. No detached flow is in evidence.

0° pitch, 6° starboard roll, shown in Figures 58, 59 and 60, show more evidence of the trailing vortex structure, even in the midships section, Figure 59. Although the roll is away from the wind, no effect is seen on the formation of any regions of detached flow.

Figures 61, 62 and 63 represent 1.1° pitch up, 6° starboard roll. The bow section, Figure 61, shows the clearest evidence yet of trailing vortices, as well as a good presentation of the flow rolling up over the port side deck edge of the flight deck. No detached flow is seen and generally smooth streaklines are visible on the midships and stern sections, Figures 62 and 63.

At this point it is noted that flow visualization was never studied in the oscillating mode of operation. The existing model weight would overload the electrical motors used to drive the oscillating mechanism. A second model, constructed of a lighter material, is being constructed but was unavailable at the time of this writing.

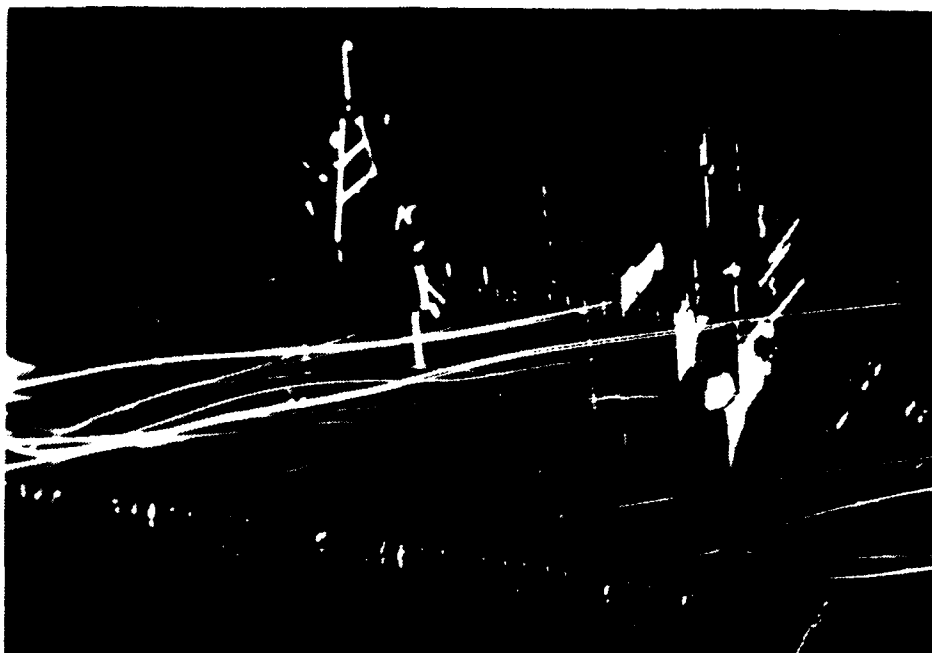


Figure 56. 30° Stbd Yaw: 1.1° Pitch Up, 6° Port Roll, Midships



Figure 57. 30° Stbd Yaw: 1.1° Pitch Up, 6° Port Roll, Stern



Figure 58. 30° Stbd Yaw: 0° Pitch, 6° Stbd Roll, Bow

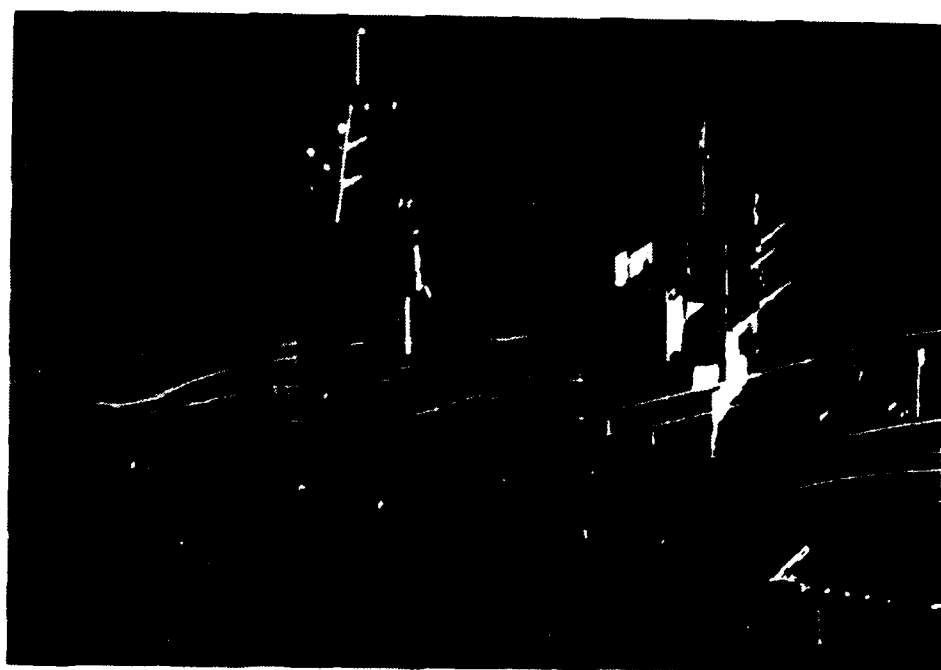


Figure 59. 30° Stbd yaw: 0° Pitch, 6° Stbd Roll, Midships

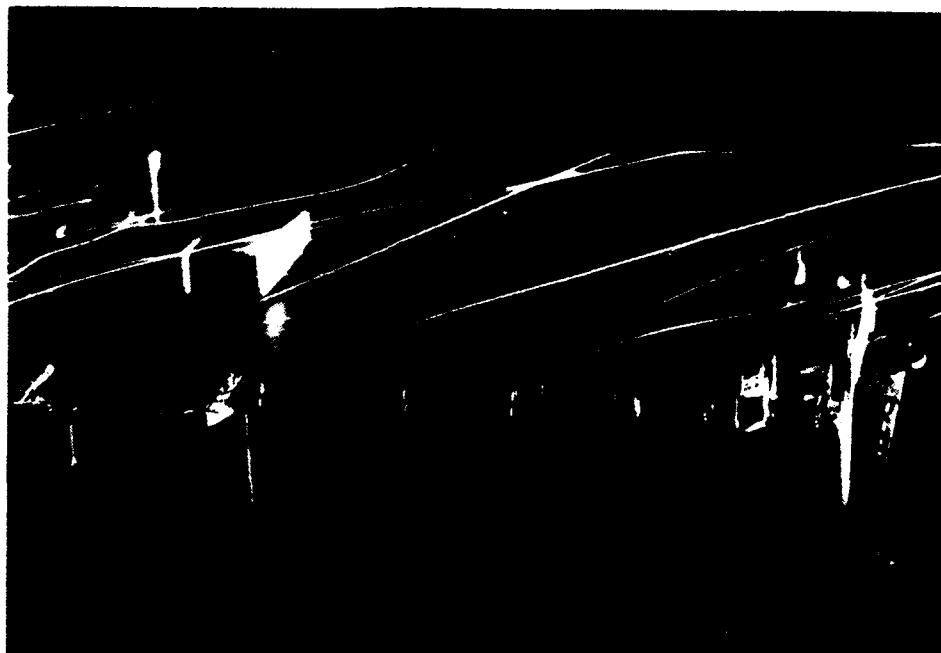


Figure 60. 30° Stbd yaw: 0° Pitch, 6° Stbd Roll, Stern



Figure 61. 30° Stbd yaw: 1.1° Pitch Up, 6° Stbd Roll, Bow

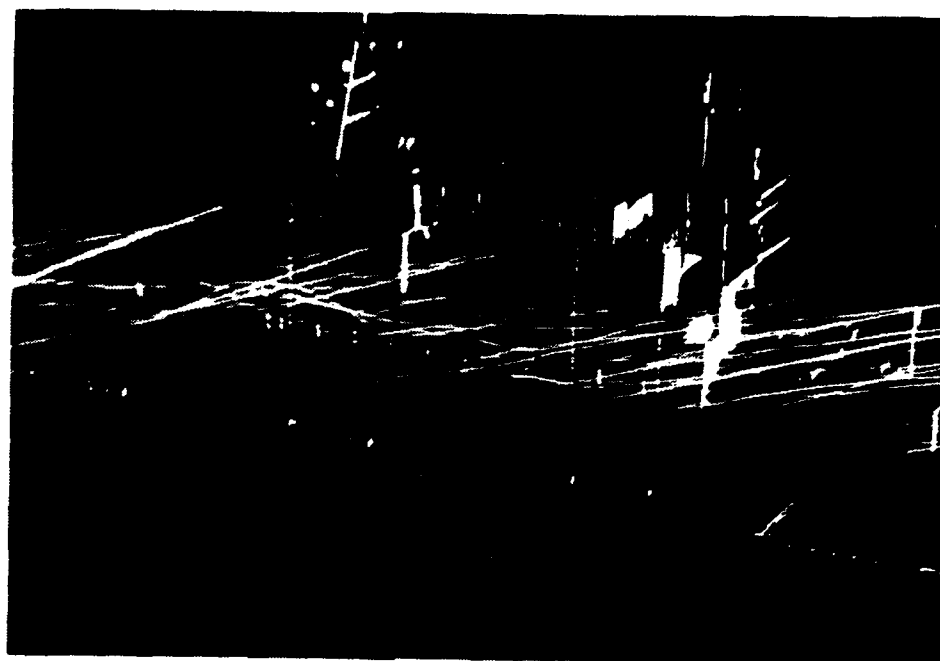


Figure 62. 30° Stbd Yaw: 1.1° Pitch Up,
 6° Stbd Roll, Midships



Figure 63. 30° Stbd Yaw: 1.1° Pitch Up, 6° Stbd Roll, Stern

VII. CONCLUSIONS AND RECOMMENDATIONS

This thesis studied the airwake around a 1:205 scale model of a TARAWA class LHA. Helium bubble flow visualization techniques were employed in a simulated atmospheric boundary layer and conducted in the environmental wind tunnel at the Naval Postgraduate School, Monterey, California. As a result of this study several basic conclusions are stated:

- 1) Helium bubble flow visualization was successful, and bubble generation was easily accomplished. Use of a second bubble "gun" cross-connected to the existing bubble generator effectively increased the swath area of the bubbles.
- 2) Use of arc lamps is clearly the best light source for helium bubble illumination. Even a cursory glance at the photographs in the Results section shows a definitive difference in illumination at the limits of the arc lamp coverage.
- 3) Light sources should be positioned so as to form parallel, or nearly parallel, ray paths. Partial image cancellation occurs when this situation is ignored.
- 4) The high vertical sides of the LHA, approximately 65 feet, do not impact on flow separation across the flight deck even at yaw angles of 45° , rather the single driving factor is the superstructure itself. Attempts at trying to cause flow separation by placing the aim point of the bubble "gun" close to the water line were unsuccessful. This bodes well for the basic hull design as a helicopter platform.
- 5) No significant amount of flow detachment and turbulence was observed for the 0° and 30° starboard yaw angles. This seems to contradict NAVAIR 00-80T-106, Appendix D, Reference 13, which highlights all helicopter spots for 30° starboard yaw angle and all spots but 3, 3A and 9 for 0° yaw angle as having

problems during flight evaluation. It should be pointed out that the near maximum wind limits were examined and that this discrepancy may not hold true at lesser wind velocities, although this would seem unlikely.

- 6) Significant amounts of turbulence, flow separation, and reversed flow regions were observed at a 45° port yaw angle. Again, Reference 13 states that all spots but 3, 3A and 9 were observed to have problems during flight envelope evaluation at this yaw angle. This study essentially verifies this with the exception of spot 9 on the stern. The stern section showed areas of reversed flow turbulence and flow separation and its suitability at this yaw angle, based on these preliminary results, is suspect.
- 7) Helium bubble flow visualization is a viable method of qualifying the airwake of a TARAWA class LHA, and serves as a starting point for quantifying the turbulence intensities of the airwake.

Based on the work done thus far the following recommendations are made:

- 1) Use of up to three additional arc lamps would provide a broader swath of illumination of the model and surrounding area. This would enable observation of the flow on both the leeward and windward sides of the model.
- 2) The second helium bubble generator has a significant helium gas leak at the console and a large bubble film leak at the vortex chamber. Upon repair of these discrepancies connecting it to two additional "guns" would allow bubble injection at a total of four points inside the tunnel. When combined with recommendation 1), this would provide a much better map of the airwake, especially at large yaw angles where greater portions of the model beam are exposed to the wind.
- 3) Enlarge the mounting platform used for placement of lights across from the control booth. This would allow the placement of arc lamps and their large collimating devices when photographing large yaw angles.
- 4) Improve the vibration isolation mountings in the tunnel so as to minimize the motion of light sources used during photography.

- 5) Speed adjustment of the wind tunnel is stiff and requires oiling.
- 6) Further analysis of yaw angles between 0° and 45° port as well as 0° and 30° starboard is required. This will serve to validate or update the envelopes as presently stipulated in Reference 13.
- 7) Use of video would allow a more detailed analysis of the subtle differences between the flow patterns at different combinations of pitch and roll at various yaw angles.

LIST OF REFERENCES

1. Arya, S.P., "Atmospheric Boundary Layers over Homogeneous Terrain," Engineering Meteorology, E.J. Plate, Editor, Elsevier Scientific Publishing Company, Amsterdam, Netherlands, 1982, Chapter 6.
2. Davenport, A.G., "The Interaction of Wind and Structures," Engineering Meteorology, E.J. Plate, Editor, Elsevier Scientific Publishing Company, Amsterdam, Netherlands, 1982, Chapter 12.
3. Healey, J. Val, "Simulating the Helicopter-Ship Interface as an Alternative to Current Methods of Determining the Safe Operating Envelopes," NPS Report 67-86-003, September 1986, Naval Postgraduate School, Monterey, California 93943-5000.
4. E.S.D.U. Data Items 74030, 74031, Engineering Science Data Unit International, Suite 200, Chain Bridge Road, McLean, Virginia 22101.
5. Garratt, J.R., "Review of Drag Coefficients over Oceans and Continents," Monthly Weather Review, July 1977.
6. Counihan, J., "An Improved Method of Simulating an Atmospheric Boundary Layer in a Wind Tunnel," Atmospheric Environment, Vol. 3, 1969.
7. Plate, E.J., "Wind Tunnel Modelling of Wind Effects in Engineering," Engineering Meteorology, E.J. Plate, Editor, Elsevier Scientific Publishing Company, Amsterdam, Netherlands, 1982, Chapter 13.
8. Biskaduros, J.L., Flow Visualization of the Airwake of an Oscillating Generic Ship Model, Master's Thesis, Naval Postgraduate School, Monterey, California, December 1987.
9. Meyers, W.G., Applebee, T.R. and Baitis, A.E., "User's Manual for the Standard Ship Motion Program, SMP," DTNSRDC/SPD-0936-01, September 1981.
10. Meyers, W.G. and Baitis, A.E., "SMP-84: Improvements to Capability and Prediction Accuracy of the Standard Ship Motion Program SMP-81," DTNSRDC/SPD-0936-04, September 1985.

11. Bolinger, W.K., Visualization of the Flow Field Around a Generic Destroyer Model in a Simulated Turbulent Atmospheric Boundary Layer, Master's Thesis, Naval Postgraduate School, Monterey, California, June 1987.
12. Bowditch, N., American Practical Navigator, H.O. Pub. No. 9, U.S. Government Printing Office, Washington, D.C., 1966.
13. U.S. Naval Air Systems Command Report NAVAIR-00-80T-106, Appendix D.
14. Naval Air Engineering Center Report NAEC-ENG-7576, 1 April 1988.

INITIAL DISTRIBUTION LIST

	No. Copies
1. Defense Technical Information Center Cameron Station Alexandria, Virginia 22304-6145	2
2. Library, Code 0142 Naval Postgraduate School Monterey, California 93943-5002	2
3. Department Chairman, Code 67 Department of Aeronautics and Astronautics Naval Postgraduate School Monterey, California 93943-5000	1
4. Commander Naval Air Systems Command Air Vehicle Division Attn: Mr. Jonah Ottensoser, Code Air 53011C Jefferson Plaza 2, Rm. 904 Washington, D.C. 20361	1
5. David Taylor Naval Ship Research and Development Center Attn: Eric Baitis, Code 1561 Bethesda, Maryland 20084	1
6. Mr. Bernard Ferrier CANDAIR LTD. 1800 Laurentieu Blvd. Saint Laurent Quebec Canada H4R1KZ	1
7. Naval Air Test Center Attn: Mr. Dean Carico, Code RW40A Patuxent River, Maryland 20670	1
8. Naval Air Test Center Attn: Mr. Jerry Higman, Code RW81 Patuxent River, Maryland 20670	1
9. Dr. J. Val Healey, Code 67He Department of Aeronautics and Astronautics Naval Postgraduate School Monterey, California 93943-5000	6

10. Mr. R.A. Feik 1
Aeronautical Division
Aeronautical Research Laboratories
506 Lorimer Street
Fisherman's Bend
Box 4331 P.O.
Melbourne, Victoria 3001
Australia
11. Ms. Susan Bales 1
Office of the Chief of Naval Operations
Navy Department
Washington, D.C. 20360-5100
12. LCDR William H. Daley, III, USN 2
5589 East Worcester Drive
Virginia Beach, Virginia 23455